Master's thesis

2020

Odin Andre Sanson

NTNU
Norwegian University of
Science and Technology
Faculty of Engineering
Department of Energy and Process Engineering

Odin Andre Sanson

Simulating Pressure Pulsations

A Future Bridge Between 1D and 3D Models

June 2020

NTNU
Norwegian University of
Science and Technology

NTNU
Norwegian University of
Science and Technology

NTNU

Norwegian University of
Science and Technology

Simulating Pressure Pulsations

A Future Bridge Between 1D and 3D Models

Odin Andre Sanson

Mechanical Engineering
Submission date: June 2020
Supervisor: Pål-Tore Selbo Storli
Co-supervisor: Celine Faudot

Norwegian University of Science and Technology
Department of Energy and Process Engineering

Summary

Fatigue loads are the primary cause of turbine failure in hydro power machinery. Cyclic loads from pressure pulsations can cause such fatigue loads. Gaining information on pressure pulsations, and the interaction between the turbine and the waterways, could be used to avoid premature failure of the turbines. The phenomenon could be studied through field measurements. However, performing and assessing measurements for a hydro power station is challenging, or can even be impossible. Accordingly, simulation tools could be utilized to gain knowledge on the behaviour of the fluid transients. A compelling option is to combine an efficient one-dimensional (1D) model with three-dimensional (3D) computational fluid dynamics (CFD) for a coupled simulation. Currently, the documentation on 1D-3D coupled models is a lacking field. The scope of this thesis the 1D model, and to investigate how a 1D-3D coupled model can be realized.

The method of characteristics (MOC) was investigated as the 1D model. MATLAB was used to code the MOC, and three different friction models were applied. Results from the literature were used to validate the models. The simulations show that transient friction must be accounted for when simulating a water hammer event in a thin pipe with a flow of a low Reynold's number. Furthermore, a newer study shows that the choice of friction model is dependent on the size and Reynold's number of the system.

To solve the problem of transferring data between the 1D and the 3D model, a 2D velocity profile was generated using the pressure gradient from the 1D MOC as the source term in the heat equation. The shape and behaviour of the velocity profiles seemed satisfactory, however, the new velocity profile did not conserve the flow rate. This error is likely related to the computed viscosity, or that the numerical solver is unable to accurately capture the sudden and large changes related to a water hammer event.

A promising method is the partly overlapped coupling (POC) technique, a non-iterative way of transferring data between the 1D MOC and 3D CFD. Due to time limitations, application of this method is outside the scope of this thesis.

The overall perception is that there is a lack of experimental data and documentation in this field. In order to further investigate 1D-3D coupled models, relevant experiments should be conducted.

Sammendrag

Utmattelsesbelastning er den primære årsaken til turbinskade i vannkraftverk. Syklisk belastning fra trykkpulsasjoner kan forårsake slik utmattelsesbelastning. Tilegning av informasjon om trykkpulsasjoner, og samspillet mellom turbin og vannvei, kan bidra til å unngå tidlig svikt i turbinene. Fenomenet kan studeres gjennom feltmålinger, men å utføre og vurdere målinger for vannkraftstasjon er utfordrende, og i enkelte tilfeller umulig. Følgelig kan simuleringsverktøy benyttes for å undersøke fluidtransienters oppførsel. Et forlokkende alternativ er å kombinere en effektiv endimensjonal (1D) modell med tredimensjonal (3D) numeriske strømningsberegninger (CFD) i en koblet simulering. Foreløpig er dokumentasjonen på 1D-3D-koblede modeller et mangelfullt område. Fokuset til denne oppgaven er 1D modellen, og å undersøke hvordan en 1D-3D-koblet modell kan realiseres.

Karakteristikkmetoden (MOC) ble benyttet som 1D modell. Den ble kodet i MATLAB, og tre forskjellige friksjonsmodeller anvendt. Modellene ble validert med resultater fra litteraturen. Simuleringene viser at transient friksjon må benyttes i simulering av et trykkstøt i et tynt rør med laminær strøm. Videre viser en nyere studie at valget av friksjonsmodell er avhengig av størrelsen, og Reynolds tallet, til systemet.

For å løse problemet med overføring av data mellom 1D- og 3D-modellen ble en 2D-hastighetsprofil generert ved å bruke trykkgradienten fra 1D MOC som kildetermen i varmeligningen. Formen og oppførselen til hastighetsprofilene virket tilfredsstillende, men den nye hastighetsprofilen bevarte ikke volumstrømmen. Denne feilen er sannsynligvis relatert til den beregnede viskositeten, eller at den numeriske løsningen ikke er i stand til å følge de plutselige og store endringene relatert til et trykkstøt.

En lovende metode, er en delvis overlappede koblings-teknikk (POC) for å overføre data mellom 1D MOC og 3D CFD. På grunn av tidsbegrensninger, er anvendelsen av denne metoden utenfor omfanget av denne oppgaven.

Den generelle oppfatningen er at det mangler eksperimentelle data og dokumentasjon på dette feltet. Veien videre i studiet av 1D-3D-koblede modeller, bør inneholde relevante eksperimenter.

Contents

Summary i

Sammendrag ii

Table of Contents v

List of Tables vii

List of Figures x

Nomenclature xi

1 Introduction 1
- 1.1 Objective & Scope . . . 2
- 1.2 Limitations . . . 3

2 General Theory 5
- 2.1 Pressure Pulsations . . . 5
- 2.2 Simulation Tools for Investigating the Transient Process . . . 6
- 2.3 Allievi's Equations . . . 6
- 2.4 Wave Propagation Speed . . . 7
- 2.5 Water Hammer Phenomenon . . . 7
  - 2.5.1 Dynamics of Water Hammer . . . 8
- 2.6 Turbulence in Pipe Flow . . . 10
  - 2.6.1 Turbulent Velocity Profile . . . 10

3 1D Models & Unsteady Friction 13
- 3.1 Relevance of Unsteady Friction . . . 14
- 3.2 Quasi-Steady Model . . . 15
- 3.3 Convolution Based Models . . . 15
- 3.4 Instantaneous Acceleration Based (IAB) Models . . . 16
- 3.5 Summary of Friction Models . . . 18

4 1D - Method of Characteristics **19**
4.1 MOC - Quasi-Steady Friction . . . 19
4.1.1 Characteristics Equations . . . 20
4.1.2 Boundary and Initial Conditions . . . 22
4.1.3 Complex systems . . . 22
4.2 Stability and Alternating Wave Speed . . . 23
4.3 MOC - MIAB Friction . . . 24
4.3.1 Characteristics Equations with MIAB Friction Model . . . 24
4.4 MOC- Zielke's Friction . . . 26

5 Concerning Coupling **27**
5.1 1D Model . . . 27
5.2 Coupling Methods . . . 27
5.3 1D to 2D; the Heat Equation . . . 29

6 Simulation Set Up **31**
6.1 Physical Set Up . . . 31
6.2 1D Simulation . . . 32
6.2.1 Quasi-Steady Friction Model . . . 32
6.2.2 MIAB Friction Model . . . 32
6.2.3 Zielke's Friction Model . . . 33
6.3 Heat Equation . . . 33
6.3.1 Turbulent Flow . . . 34

7 Results & Discussion **37**
7.1 1D MOC Simulations . . . 37
7.1.1 Quasi-Steady Model . . . 38
7.1.2 MIAB Model . . . 38
7.1.3 Zielke's Model . . . 39
7.1.4 Discussion; 1D friction models . . . 40
7.2 Heat Equation for a 2D Velocity Profile . . . 42
7.2.1 Steady State Simulation . . . 42
7.2.2 Transient Simulation . . . 43
7.2.3 Comparing Flow Rate to Original MOC . . . 45
7.3 Turbulent Velocity Profile . . . 50
7.4 Discussion . . . 53
7.4.1 Heat Equation as Translator . . . 53
7.4.2 Relevance of unsteady friction . . . 53
7.4.3 Coupling & Notion Towards Further Work . . . 54

8 Conclusion and Further Work **55**
8.1 Further Work . . . 56

Bibliography **57**

Appendix A **I**

Appendix B **IX**

Appendix C **XII**

Appendix D **XIV**

Appendix E **XXVI**

Appendix F **XXIX**

List of Tables

7.1 Seconds CPU-time of the different friction models used with the MOC . . 40

List of Figures

2.1 A simple system with a pipe connecting a reservoir and a valve 7
2.2 The changes of a velocity profile as a water hammer pressure pulse passes a section 8
2.3 Transient pressure adjacent to the closed valve during a water hammer, modelled with no friction 9
2.4 Transient pressure during a water hammer, modelled with a transient friction model 9
2.5 Laminar and turbulent pipe flow 10

4.1 The characteristic lines in the xt plane 20
4.2 The grid used with MOC and MIAB friction model 25

5.1 Illustration of **(a)** Adjacent Coupling (AC) and **(b)** Partly Overlapped Coupling (POC) 28

6.1 Illustration of Bergant's experiment, taken 31

7.1 MOC with Quasi-Steady friction model vs experimental results 38
7.2 MOC with MIAB friction model vs experimental results 39
7.3 MOC with Zielke's friction model vs experimental results 39
7.4 Convergence of center velocity 42
7.5 Velocity Profile 43
7.6 Transient velocity profile from $t = 0.0225s$ to $t = 0.0451s$ 44
7.7 Transient velocity profile from $t = 0.0789s$ to $t = 0.101s$ 44
7.8 Transient pressure of the same node as the velocity profile in Figure 7.6 and Figure 7.7 45

7.9 **(a)** shows flow rates for MOC (QS) and the respective heat equation. The flow rates are normalized by the initial, steady state flow rate Q_0 **(b)** shows the difference in flow rates between MOC and the heat equation for various friction models. The flow differences are normalized by the same initial, steady state flow rate Q_0 Both figures are related to a node located $0.074m$ from the outlet 46
7.10 Difference in flow rate between the heat equation and the MOC (QS) divided by the initial flow rate, for a variation in time step 47
7.11 Relative flow rate of the flow obtained using the heat equation and the MOC with Zielke's friction model 47
7.12 Relative flow rate of the flow obtained using the heat equation and the MOC with Zielke's friction model, zoomed in 48
7.13 Viscosity Relative to position from center 50
7.14 Velocity change at the center of the pipe cross-section 51
7.15 Comparing velocity profile constructed with heat equation and power law of $n = 7$ 52

A1 The grid used with MOC and MIAB friction model III
A2 Illustration of the offset of H'_P compared to H_P V
A3 Illustration characteristic lines from offset H values V
A4 Illustration of upstream boundary mismatch, displacement of characteristic line C^- VII
A5 Illustration of downstream boundary mismatch, and quantities for interpolation VIII
B1 Series Connection IX
B2 Branched junction X
F1 Freebody diagram showing the forces acting on a control volume XXIX

Nomenclature

ν	Kinematic viscosity, $[m^2/s]$
ϕ	Sign-correcting coefficient, $[-]$
τ	Dimensionless number describing the discharge coefficient times area opening at a valve
A	Cross-sectional area of pipe, $[m^2]$
a	Wave propagation speed, $[m/s]$
A^*, B^*	Parameters in the weighting function, ref Zielke's model, $[-]$
B	Allievi constant $a/(gA)$, $[s/m^2]$
C^+, C^-	Name for characteristic equations
C_P, C_M	Coefficients in characteristics equations
C_r	Courant number, $[-]$
D	Pipe diameter, $[m]$
E_m	Exponent of τ-equation, $[-]$
f	Darcy-Wiesbach friction coefficient, $[-]$
g	Gravitational constant, $[m/s^2]$
H	Piezometric head, $[m]$
h_f	Head loss per unit length, $[-]$
H_{sub}	Piezometric head at point specified by subscript, $[m]$
k	Friction coefficient in IAB model, $[-]$
k_t	Friction coefficient related to temporal derivative, $[-]$

k_x	Friction coefficient related to spatial derivative, $[-]$
L	Pipe length, $[m]$
M	Mach number, $[-]$
Q	Average discharge at a section, $[m^3/s]$
Q_{sub}	Average discharge at point specified by subscript, $[m^3/s]$
R	Resistance coefficient
t	As subscript denotes partial differentiation
t	Time variable, $[s]$
t_c	Closing time of a valve, $[s]$
u	Convolution integral time-variable
V	Bulk flow velocity, $[m/s]$
W	Weighting function
x	As a subscript denotes partial differentiation
x	Distance along pipe, $[m]$
1D	One-dimensional
3D	Three-dimensional
AC	Adjacent Coupling
CB	Convolution Based
CFD	Computational fluid dynamics
CFL	Courant-Friedrichs-Lewy
IAB	Instantaneous Acceleration Based
MIAB	Modified Instantaneous Acceleration Based
MOC	Method of characteristics
NS	Navier-Stokes
POC	Partly Overlapped Coupling
QS	Quasi-steady
RSI	Rotor stator interaction
WFB	Weighting function based

Chapter 1

Introduction

Pressure pulsations, often referred to as fluid transients, in hydro power machinery are a well known phenomena. Such pulsations may lead to waterway resonance and fatigue loads (cracks) on the turbine.

Usually, pressure pulsations are generated at the runner or in the draft tube. Due to the compressible nature of water, the pressure pulses will propagate in the waterways until reaching a reflection point and then return to the runner. This interaction between the waterway and the turbine is of peculiar interest, and is the basis of this study. Ideally, one would use experimental results to investigate this interaction, however it can be difficult to obtain data as it may be troublesome to mount measurement equipment on large hydropower units. Even if measurements are conducted, they may be difficult, or even impossible to assess as usually a large amount of noise is present. As a part of an ongoing research project called *Fatigue Loads in Hydro Turbines*, transient behaviour at Kvilldal hydropower station was investigated. Large amounts of noise in the measurements rendered the report inconclusive [1]. Hence, strong and reliable simulation tools could provide insightful information on the behaviour of pressure pulsations, and how they cause harm.

Several ways of numerically approximating transient fluid flow exist. Generally, three-dimensional (3D) computational fluid dynamics (CFD) fully simulates fluid flow, and account for both transient and 3D effects. However, the accuracy of 3D CFD comes at a large computational cost. Fully modelling both turbine and conduits with 3D CFD is simply unfeasible and unnecessary. One-dimensional (1D) models have proven to be both accurate and efficient for modeling transient events in water conveying systems where the axial forces are dominating, such as pipe flow. In particular, the 1D Method of Characteristics (MOC) is a widely used and documented method which is developed to model transient events in pipe flow. Therefore it may be useful to divide the simulation into a 1D and a 3D model.

Coupling the 1D MOC with 3D CFD will reduce the computational time, and could prove to be an insightful way of studying how pressure pulsations from the runner interact with the waterway. Consequently, issues related to a 1D-3D coupled model needs to be

concerned. The primary issues are listed underneath.

- The friction model used with the 1D MOC

For certain transient events, it may be challenging to compute the frictional loss in a 1D model. Yet, there are ways of estimating the transient friction to high precision. Choosing the correct friction model is necessary for the model to be accurate.

- How to realize the coupling between the 1D and 3D model

Coupled simulations is a relatively new field of study. Consequently, there is little documentation in the literature. The way information is transferred between the models will largely impact the results.

- How to add compressibility to the 3D CFD model

3D CFD is usually simplified by assuming water is incompressible. However, the propagation of pressure pulsations is a consequence of the compressibility, and has to be accounted for in the model.

1.1 Objective & Scope

The objective of this thesis is to investigate elements related to a 1D-3D coupled model. Both 1D and 3D simulations are large fields of study by themselves, and all the aspects will not be concerned in this work. The focus will be on the 1D model and how the flow variables are transferred between the 1D and 3D model.

For the purpose of investigating the 1D model, a water hammer simulation will be performed by using the 1D MOC. There are several ways of computing the transient friction in the MOC. How the frictional loss is computed in a 1D model will affect a potential 1D-3D coupled model. To study the effects of transient friction, three different friction models will be applied and validated against an experiment and simulations performed by Bergant et al. [2]. Additionally, a literature study investigating transient friction will be performed.

One of the main concerns in a 1D-3D coupled simulation is how to transfer the flow variables between the models. A literature study will be conducted to investigate coupling techniques.

Storli[1] suggested an interesting technique for producing a 2D velocity profile, using the pressure gradient from the 1D MOC. The 2D velocity profile is computed from a reduced version of the Navier-Stokes (NS) momentum equation, on the form of the heat equation. This could prove to be a useful technique for coupling 1D and 3D models and will be investigated as part of this work.

All the work done is carried out with a coupled model in the back of the mind. Hopefully, it will serve as a stepping stone for future work in this field, and illuminate certain critical considerations when modelling transient events in pipe flow.

[1] This method is not documented in the literature. Storli used the technique in a presentation at the 24th IAHR Symposiom in Brazil 2008. The presentation was related to a publication by Storli and Nielsen [3].

1.2 Limitations

Initially, ANSYS Twinbuilder was suggested for the purpose of creating a 1D-3D coupled model. A license for this program was obtained after a long and tedious process. Unfortunately, the program could not work directly with CFD, and so it was unfit for the sake of this work. Twinbuilder is a program based on Reduced Order Models for more efficient simulations, and it is not in the scope of this study.

The CEL language, available in ANSYS CFX, appeared to be a viable option for setting up a 1D-3D coupled model. However, this was realized too late to be applied in this work.

Chapter 2

General Theory

2.1 Pressure Pulsations

Pressure pulsations are disturbances propagating in the fluid domain, affecting the pressure and flow rate of the system. They are caused by a continuously oscillating discharge pressure, causing a non-steady pressure and flow to propagate in the waterways. The response of the water conduit may be seen as a dependency between the pressure pulsation and the flow pulsation. In such a way, the behaviour of pressure pulsations is governed by three types of properties [4].

- Fluid inertia
- Compressibility
- Dissipation (friction)

During the operation of a Francis turbine, pressure pulses may be caused by a swirling flow phenomenon, such as the draft tube vortex phenomena, or runner-casing interaction such as rotor stator interaction (RSI). Another type of transient is the water hammer phenomenon. This is a severe transient event, however it is relatively easy to set up in an experiment and provides useful comparison for the simulation models which will be presented in this work.

High frequency pulsation phenomena may cause strong vibrations in the mechanical structures of the runner, possible causing fatigue or failure in the mechanical components. For example, RSI between runner blades and and inlet has been known for a long time to cause runner failures or structural vibrations. Adequately simulating these phenomena could provide insightful information, which could prevent harmful pulsations during the operation of the runner.

2.2 Simulation Tools for Investigating the Transient Process

For the sake of this work, modelling the fluids in hydraulic machinery is divided into two parts, 1D models and 3D models.

The 1D models can provide an accurate description of the fluid in areas where the flow is governed by axial forces, for example in long pipe sections. The Method of Characteristics (MOC), developed by Wylie and Streeter [5], is such a method and will be thoroughly described in chapter 4. Provided the wave propagation speed is known, the 1D model can accurately simulate transient events in areas where 1D assumptions are valid.

The 3D CFD model is based on numerically solving the Navier-Stokes (NS) equations. They are set up to model the fluid across three dimensions, providing a detailed and accurate simulation tool at the expense of substantial computational resources. Commonly, simplifications are used to make the simulation more efficient, such as the assumption of incompressible fluid. However, the assumption of incompressibility cannot be used when modelling pressure pulsations, and a compressibility model is needed. How to model pressure pulsations using a 3D CFD model is presented in Appendix C, since it is not the scope of this thesis.

Currently, the main limitations of 3D CFD is related to large computational cost. Model order reduction (MOR) is a way of reducing the computational cost, and still provide accurate simulations. Details on MOR and how to handle the 3D simulation in a coupled model is added in Appendix C.

2.3 Allievi's Equations

Allievi's equations are often referred to as the governing equations for pipe flow. The derivation of these equations, adopted from Wylie and Streeter [5], can be found in Appendix F. These equations are derived based on simplifications justified by the following assumptions.

- The fluid is of a low compressibility.
- The convective acceleration terms are negligible as the velocity is much lower than Mach number unity.

Following these assumptions leads to Equation 2.1 and Equation 2.2. The method of characteristics (MOC) solves these equations to compute the transient properties of pipe flow. MOC will be thoroughly described in chapter 3.

$$gH_x + V_t + f\frac{V|V|}{2D} = 0 \tag{2.1}$$

$$H_t + \frac{a^2}{g}V_x = 0 \tag{2.2}$$

g is the gravitational constant, H is the piezometric head, the subscripts $_x$ and $_t$ denotes the spatial and temporal partial derivative respectively, V is the bulk flow velocity, f is the Darcy-Weisbach friction factor and a is the wave propagation speed.

2.4 Wave Propagation Speed

The speed of a disturbance propagating in water is easily described in terms of the density ρ and the modulus of elasticity (sometimes referred to as bulk modulus") K.

$$a = \sqrt{\frac{K}{\rho}} \tag{2.3}$$

Using a density of $\rho = 1000kg/m^3$ and a modulus of elasticity of $K = 2.1GPa$ gives a wave speed of $1449m/s$, the normal speed of sound in water. However, the wave speed in pipes or other waterways are effected by several other factors, such as the elasticity of the wall and the presence of air. A steel penstock in a medium-head plant would commonly have a wave speed around $1000m/s$ [4].

When modelling and investigating pressure pulsations, using the correct wave speed is crucial. For pipes in controlled environments the analytical wave speed usually is accurate. However, controlling everything quickly becomes difficult, even on a test bench. In hydro power stations, there may be several factors affecting the wave speed, making it difficult or impossible to predict. Perkunder et al. [6] applied a technique used in seismology called *Seismic Interferometry*, to measure the wave speed. The technique proved successful when tested in an experiment at *NTNU's Hydropower Laboratory*. It was later attempted on a large hydropower station with four parallel Francis runners. Unfortunately, too much noise in the measurements rendered the method inconclusive.

2.5 Water Hammer Phenomenon

Water hammer is a phenomenon caused by sudden and complete closure of a valve downstream in a pipe, located as seen in Figure 2.1. The sudden closure stops the flow completely adjacent to the valve. There is still flow in the pipe which causes a large rise in pressure travelling upstream with the speed of sound. An increase in pressure and a bulk flow of zero will be trailing the pressure wave. Eventually, the wave front reaches the reservoir. At this point, the pressure in the pipe exceeds the pressure of the reservoir, and back flow will occur. A new pressure front will then travel downstream, trailed by a negative velocity. This pressure will propagate between the reflection points of the pipe, possibly causing serious harm to the hydro power station.

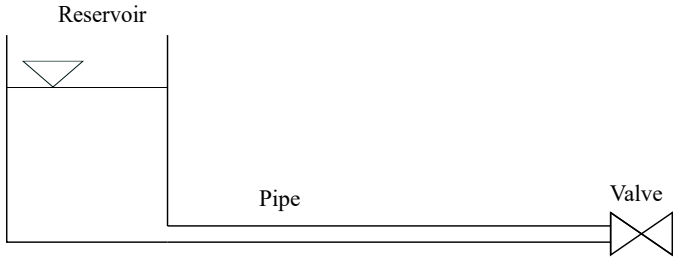

Figure 2.1: A simple system with a pipe connecting a reservoir and a valve

Some important properties related to the water hammer is listed below.

- $T_r = \frac{2L}{a}$
  T_r, the reflection time, is the time it takes for the pressure wave to travel from the valve, to the reservoir and back.

- $\Delta p = \rho a \Delta v$
  Δp is the Joukowsky pressure, and it is the maximum pressure achievable, for the given conditions.

- If the closing time T_L of the valve is less then the reflection time T_r, Joukowsky pressure will be reached, and there will be a water hammer event.

In the industry, water hammer is a worst case scenario and needs to be avoided. This is done by altering the reflection points or the closing time of the downstream valve. One does not necessarily need to run advanced simulations, including for example transient friction, when dimensioning a hydro power station to prevent this. A transient friction model may even lead to underestimating the pressure amplitudes. The main concern is to avoid the worst case scenario. For this purpose a simple model, utilizing a quasi-steady friction model, is usually sufficient.

Although an advanced friction model may be unnecessary for predicting the main features of a water hammer in a hydro power station, it may have an impact on a 1D-3D coupled model. Various types of friction models and their use will be discussed in chapter 3.

2.5.1 Dynamics of Water Hammer

When the valve is shut and the pressure wave is travelling upstream, the bulk flow trailing the pressure will be approximately zero. Hence, the mean velocity and acceleration will be zero until the pressure wave returns. However, the velocity profile will still be present. It is pushed back by the pressure wave in a way that results in large gradients near the wall, as seen in Figure 2.2, resulting in a large skin friction.

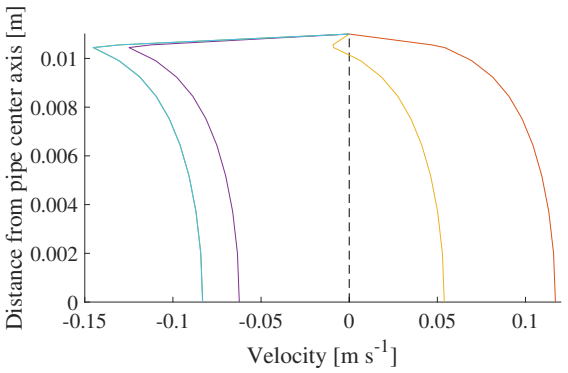

Figure 2.2: The changes of a velocity profile as a water hammer pressure pulse passes a section

Frictional forces are computed from the shear stress, which is defined from the velocity gradient.

$$\tau = \mu \frac{du}{dr} \tag{2.4}$$

The added contribution from the time varying friction is easily understood and computed in 2 dimensions. It is however more problematic to implement in a 1D model only utilizing the section average flow, i.e. no velocity gradient. However, as the 2D and 3D models tend to demand extensive computational resources, modelling the effects from transient friction in 1D models has been extensively studied. Details on 1D models accounting for transient friction will be presented in chapter 3.

The added frictional contribution have effects on attenuation of the pressure amplitude and the wave shape for flow with a low Reynolds number in thin pipes. In addition, the transient pressure, just upstream of a closed valve during a water hammer event, may take on a slightly different form, depending on the choice of friction model [2, 7]. If transient friction is not accounted for, the friction will have squared peaks, as seen in Figure 2.3.

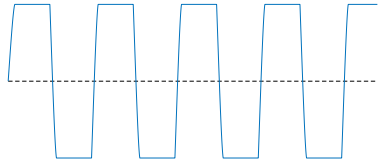

Figure 2.3: Transient pressure adjacent to the closed valve during a water hammer, modelled with no friction

Several ways of modelling transient friction have been developed. These types of methods will compute the head loss differently which in turn will attenuate the pressure amplitudes. In addition, shape of the pressure wave and plot may vary depending on the friction model chosen. A transient pressure plot is illustrated in Figure 2.4. Note how the peaks have less of a square shape than in Figure 2.3, where transient friction is not accounted for. A study by Martins et al. [7] shows that the pressure plot from a 3D CFD model will have a better match with the 1D model accounting for transient friction.

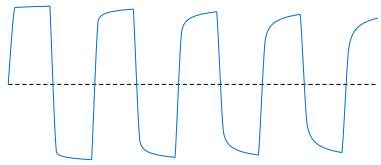

Figure 2.4: Transient pressure during a water hammer, modelled with a transient friction model

2.6 Turbulence in Pipe Flow

Due to the large pipes and high flow velocities in hydro power stations, turbulent effects are generally present. The randomness of turbulence makes numerically approximating flow properties even more complicated. Several semi-empirical models have been developed in order to provide closure to the equations of motion when accounting for turbulent stresses. In some of the simpler turbulence models, the viscosity is modified in order to obtain a more convenient representation of the turbulent shear stress. This was first introduced by the French mathematician Joseph Boussinesq. The total shear stress when using eddy viscosity to represent the turbulent shear has the following mathematical representation [8].

$$\tau_{total} = (\mu + \mu_t)\frac{\partial \bar{u}}{\partial y} \tag{2.5}$$

μ_t is the eddy viscosity and $\bar{u}$ is the average velocity. Using this concept is very appealing, however, it is of no practical use unless the eddy viscosity can be determined.

Eddy motion and thus eddy diffusivity is much larger in the core region of a turbulent boundary layer. Closer to the wall, the eddy motion loses its intensity, and diminishes at the wall due to the no-slip condition. Note, the molecular diffusivity of momentum is a fluid property. Eddy viscosity, however, is dependent on the flow conditions. The value of the eddy viscosity increases from zero at the wall to several thousand times the molecular diffusivity in the core region [8].

2.6.1 Turbulent Velocity Profile

The expressions for turbulent velocity profiles are semi-empirical as they are based on both empirical and analytical considerations. For pipe flow, u normally denotes the time-averaged velocity in the axial direction. For laminar flow, the streamlines will be parallel to the pipe wall, making it easier to analyze the flow. For turbulent flow, the streamlines take on a more chaotic form, illustrated in Figure 2.5. Providing a mathematical representation of the full turbulent region has proven to be difficult.

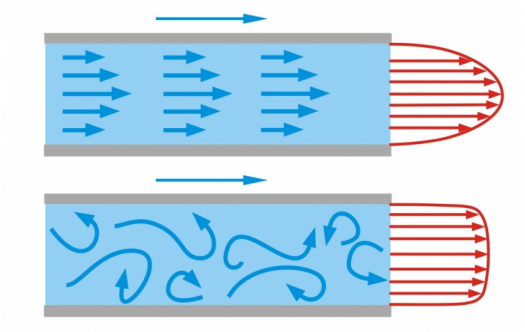

Figure 2.5: Laminar and turbulent pipe flow

A non-dimensional analysis provides two equations, known as *law of the wall* and *the universal velocity profile* for turbulent flow. Neither is able to model the full flow region. In addition there is a buffer layer between the region close to the wall, and the outer flow region where neither of the models are accurate.

There are numerous empirical velocity profiles exist for turbulent pipe flow. A simple and well-known method is the **power-law velocity profile**. It is represented mathematically by the following equation.

$$\frac{u}{u_{max}} = \left(1 - \frac{r}{R}\right)^{1/n} \tag{2.6}$$

In the above, r is the position from the pipe center and R is the radius of the pipe. The value of n increases with increasing Reynolds number. The value $n = 7$ approximates many flows in practice which has even given rise to the term *one-seventh power-law velocity profile*. When n increases, the velocity profile becomes fuller, i.e. flatter, with steeper gradients near the wall.

The maximum velocity over a cross-section can be determined from the section average velocity, $\bar{u}$.

$$u_{max} = \bar{u}\frac{(n+1)(2n+1)}{2n^2} \tag{2.7}$$

The power-law profile cannot be used to compute the wall shear stress since it gives a velocity gradient of infinite at the wall ($r = R$). In addition, the profile fails to give a zero slope at the center of the pipe. Despite those discrepancies, it provides a quite accurate overall presentation of the velocity profile, which can be useful when evaluating other methods for producing a turbulent velocity profile [8].

Chapter 3

1D Models & Unsteady Friction

The long-term objective of this work is to completely simulate transient events in hydro power stations with complex waterway and multiple runners. For the model to accurately replicate certain real-life events, the friction model in the 1D simulation may be of critical importance. Sections 3.2 to 3.4 presents different models constructed for handling transient friction. In section 3.1, a literature study on the relevance of transient friction models is presented.

Many existing models approximating transient friction are constructed based on laminar flow assumptions. The friction models based on laminar flow can be validated and improved when tested against experiments with laminar flow conditions, i.e. smaller pipes and lower velocities.

For the sake of validating a model, it is favorable to have experimental results for comparison. For example, when validating of a coupled model. Measurements from hydro power stations are often polluted with noise, making them difficult to interpret. Smaller experiments are less expensive, and provide results which are more easily assessed. Note that the choice of friction model may depend on the size of the system, and type of transient event. Several studies show that transient friction has to be accounted for in simulation of a water hammer in a thin pipe with a low Reynolds number [2, 9, 10, 11, 12, 13]. Thus, a transient friction model should be utilized for a qualitative comparison with such an event.

3.1 Relevance of Unsteady Friction

In the literature, there are several studies substantiating the importance of transient friction in order to precisely simulate transient phenomena [2, 9, 10, 11, 12, 13, 14, 15]. However, the small pipes of experimental set ups, and the nature of the severe transients evaluated, may have led to overestimating the importance of a transient friction model [16]. Even though several unsteady friction models provide excellent fit compared to experimental results, there are some issues that need to be considered. This project has the long term goal of improving the simulation of transients in the waterway of hydro power stations, and it is important to note that a hydro power station is of a completely different scale than most experiments used for validating the 1D friction models.

Stephens et al. [17] compared a 1D the model to field tests in order to assess the contribution of unsteady friction. For lower Reynolds numbers, the unsteady friction model improved the performance considerably. However, the contribution from the unsteady friction model was reduced with a higher Reynolds number.

The impact of the system scale has been evaluated in a study by Duan et al. [16]. The authors were able to relate the relevance of the unsteady friction to system scale L/D, the quasi steady shear stress f, the Reynolds number Re and the Mach number M. As the product $f \times Re$ increases, the importance of the dampening from unsteady friction models is reduced. Unsteady friciton also becomes less significant as L/D increases. Duan et al. came up with the criterion that for $fML/D > 0.1$, an unsteady friction model has little to provide other than increased computational time. Note that this conclusion is drawn for a system subjected to a sudden and complete valve closure causing a water hammer. This is the most severe transient event, causing back flow and steep velocity gradients close to the walls. For more complex systems exposed to milder transients, the criterion is probably less than 0.1 [16].

For the sake of validating a coupled method, and evaluating how the 1D and 3D model communicate, comparison with experimental results can be insightful. Most of the experiments and simulations are for water hammer events in in small pipe systems. Diameters in the range of tens of millimeters and pipe length in tens to hundreds of meters. This necessitates the use of an unsteady friction model.

Another notable observation is that several friction models may model wave attenuation and phase of the pressure wave correctly. However, the wave shape may be affected by the choice of unsteady friction model [7]. In 3D CFD simulations the wave front takes a characteristic S-shape [18]. In the coupled model this may prove significant and affect the choice on how to model the friction in the 1D section.

Governing Equations

The governing equations, also referred to as Allievi's were presented in section 2.3, and are repeated below.

$$H_x + \frac{1}{g}V_t + h_f = 0 \tag{3.1}$$

$$H_t + \frac{a^2}{g}V_x = 0 \tag{3.2}$$

H is the piezometric head, the subscripts $_x$ and $_t$ denotes the spatial and temporal partial derivative respectively, g is the gravitational constant, V is the bulk flow velocity, h_f is the head loss per unit length and a is the wave propagation speed.

In transient events with rapid velocity changes and large velocity gradients, the velocity profile near the wall will undergo dramatic variations with possible flow reversal. This notable and rapid change in the velocity profile will affect the friction. In order to account for the unsteady friction, the head loss h_f is divided into a quasi-steady term $h_{f,q}$, and an unsteady term $h_{f,u}$

$$h_f = h_{f,q} + h_{f,u} = f\frac{V|V|}{2gD} + h_{f,u} \tag{3.3}$$

f is the friction coefficient and D is the internal pipe diameter.

Above, the quasi-steady term is determined using the Darcy-Weisbach friction model. Computing the unsteady term in an efficient and yet precise way is difficult. Subsequently three methods for computing the unsteady term will be described, as presented by Storli [9]. Storli and Vítkovskỳ et al. will be extensively cited in this section [9, 10].

3.2 Quasi-Steady Model

The quasi-steady (QS) model is the simplest of the models presented in this work. Neglecting the unsteady term, $h_{f,q}$, the frictional loss is purely computed by the Darcy-Weisbach formula.

$$h_f = h_{f,q} = f\frac{V|V|}{2gD} \tag{3.4}$$

Losses are computed purely from the section average velocity. This implementation is fast and efficient. In addition, it is included for all the models. For upcoming models, it will be added together with an unsteady term, $h_{f,u}$.

In certain events, this model may be insufficient. Head loss is computed purely from the instantaneous section-average flow velocity. It does not account for the velocity gradient, or the rate at which the velocity is changing.

3.3 Convolution Based Models

The Convolution Based (CB) models are based on the past history of bulk accelerations. The name is given as the accelerations are applied in a convolution integral. Initially, the model was developed by Zielke (1968). Since the original model require extensive

computational time, the model has been subjected to modifications in order to reduce the computational demand. Trikha [19] improved speed at the expense of accuracy, Kagawa et al. [20] and Suzuki et al. [21] created implementations with both high accuracy and high computational efficiency. Vardy and Brown [12] determined a set of weighting functions for the CB approach for smooth pipe turbulent flows. This model has been further improved and is referred to as the weighting function based (WFB) model. More recently, Ghidaoui and Mansour [22] were able to implement Vardy-Brown weighting function with the method of characteristics (MOC), as cited by Vítkovskỳ et al. [10]. The initial model developed by Zielke is presented below.

$$h_{f,u} = \frac{16\nu}{gD^2} \int_0^t \frac{\partial V}{\partial t}(u) W(t-u) du \tag{3.5}$$

W is the weighting function, ν is the kinematic viscosity and u is the convolution time.

Typically, the simplifications consists of approximating the weighting function W, by exponential functions. The WFB model has also been modified to be valid for smooth pipe flow in the turbulent regime by several researchers [23, 22, 12]. As formerly stated, many hydro power stations, such as Kvilldal, will have turbulent flow. Hence, it is crucial that the friction model in the simulation is valid for turbulent flows.

A great advantage of WFB models is that they are not dependent on coefficients that must be established in some way. Instead, it is based on physical considerations, making the model generally applicable for fluid transients. However, the WFB model shows less accuracy for continuously accelerating and decelerating flows, such as the water hammer event [10, 9].

A study performed by Duan et al. [16] shows that since the WFB model implements the flow history, it is able to resemble the shape of wave. In a transient pressure plot, a steady state friction model will have approximately horizontal amplitudes at the Joukowsky pressure level. The WFB model will reach a pressure of $90 - 95\%$ of the Joukowsky pressure and then increase towards 100% before it drops. Martins et al. [7] compared the WFB model to a CFD model, and the study shows that the two models produce closely matching wave shapes. This could prove to be relevant when constructing a coupled model.

3.4 Instantaneous Acceleration Based (IAB) Models

Instantaneous Acceleration Based (IAB) models, fathered by Daily et al. [24] and further modified and improved by Golia [25], Brunone et al. [26] and Bergant et al. [2], are computationally fast and easy to implement. However, the models are dependent on one or two coefficients that need to be determined in order to correctly compute the friction. The coefficients are normally calibrated using experimental results. A mathematical representation of the single coefficient unsteady friction model is presented subsequently [9, 10].

$$h_{f,u} = \frac{k}{g}\left(\frac{\partial V}{\partial t} - a\frac{\partial V}{\partial x}\right) \tag{3.6}$$

In Equation 3.6, k is the friction coefficient. When using an IAB model with a single coefficient, the coefficient has been determined in various ways. It has been found from

experimental results, analytical relations, and post calculated from more complex models, such as Zielke's CB model [27, 28, 11].

The IAB model has been further modified to include two coefficients, one for each of the derivative terms. This introduces two coefficients to be determined, k_t and k_x, and the new equation becomes

$$h_{f,u} = \left(\frac{k_t}{g} \frac{\partial V}{\partial t} + \frac{k_x a \phi}{g} \frac{\partial V}{\partial x} \right) \tag{3.7}$$

A new coefficient, ϕ, is introduced to modify the equation to provide the correct sign of the dampening for every position of the valve in the system. It is defined as

$$V \frac{\partial V}{\partial x} \geq 0 \qquad \Rightarrow \qquad \phi = 1$$
$$V \frac{\partial V}{\partial x} < 0 \qquad \Rightarrow \qquad \phi = -1$$

This representation of the head loss has shown to potentially give a more general representation of experimental results [9, 29]. Generally, the model represented by Equation 3.7, is referred to as the Modified Instantaneous Acceleration Based (MIAB) model.

Analyzing the model has shown that the two different derivative terms are responsible for different behavior. The spatial derivative is responsible for dampening, and the temporal derivative is exclusively involved in phase shifting [10].

Vítkovskỳ et al. [10] found that although the MIAB model gives a good representation of valve closing events, it does not work well for valve opening events. A possible explanation for this may be attributed to unrealistic choice of coefficients rather than a general failure of the model. However, if the MIAB model is to be improved, it is probable that the coefficient cannot be independent of time [9].

Storli and Nielsen [30] investigated the MIAB model using coefficients which vary along the pipe length. The coefficients were determined based on the more complex and accurate CB model. When compared to experimental results, the model showed good agreement for Reynolds numbers of 2000 and 5800. However, the improvement of the model was not general, but was only valid for for complete closure of a downstream valve in a single pipeline at low Reynolds numbers.

Duan et al. [31] did an analytical analysis on IAB and WFB. In conclusion the IAB model was able to better predict the transient envelope attenuation than the transient evolution phase shape. Similar results were found by Martins et al. [7] when comparing the two friction models to a CFD simulation. Overall, the WFB model provided better fit with CFD results.

Once again, this may prove essential when setting up the coupled model. The IAB and MIAB models are computationally faster and require less memory use than the WFB model. However, in the set up of a coupled 1D-3D model, the difference between the models may cause added numerical error or even spurious transients. Evaluating what 1D friction model to use will depend on the type of flow, and the scale of the system.

3.5 Summary of Friction Models

The pros and cons of the friction models presented in this section are briefly listed below.

- **Quasi-steady**
  - The fastest of the models discussed in this chapter.
  - The computational memory required is small, and only dependant the number of reaches the pipe is divided in.
  - Fails to model attenuation and phase shift of the transient pressure head during a water hammer event, for laminar flow in a thin pipe.
  - No coefficients need to be determined.
- **MIAB**
  - Not as fast as QS, but still a relatively fast model.
  - The amount of computational memory required is slightly more than the QS model, but very close.
  - Successfully models attenuation and phase shift of the transient pressure head during a water hammer event, for laminar flow in a thin pipe.
  - This method poses the need for interpolation, which adds another possible source of numerical error
  - Friction coefficients needs to be determined, either from other models or experiments.
- **Zielke**
  - This requres the most CPU time of the models presented.
  - The memory load from this model may be very large, and it is proportional to how long the simulation run for and how small the time step is
  - Successfully models attenuation and phase shift of the transient pressure head during a water hammer event, for laminar flow in a thin pipe.
  - No need for interpolation or coefficients to be determined.

How the choice of friction model will impact a 1D-3D coupled model has not been studied. The literature unequivocally consents that a transient friction model is required for water hammer events in thin pipes with a low Reynold's number. For such events, a coupled model would be affected by the choice of friction model in the 1D segment, as such all the 1D models presented will be utilized. In addition, a 3D CFD simulations with a sufficiently fine mesh, also take on the same characteristics for these type of events.

As stated in section 3.1, the relevance of a transient friction model diminishes as the scale of the pipe and Reynold's number increases. If one were to set up an experiment to investigate coupled simulations in NTNU's hydro power laboratory, the friction model would have to be considered separately before a coupled simulation could be conducted. In addition, the nature of the water hammer phenomenon may also lead to overly estimating the need of a transient friction model. Additional experiments with less severe transient events than a water hammer could be useful, as the long term goal is to simulate a hydro power station under operating conditions, and not water hammer events.

Chapter 4

1D - Method of Characteristics

The partial differential equations governing unsteady fluid flow in pipelines does not have a general solution. The equations can be transformed by the Method of Characteristics (MOC) into total differential equations, which are integrated yielding finite difference equations which are conveniently handled numerically.

MOC is by far the most used method. The method is accurate, efficient and is simple to implement, which is the reason for its popularity [13]. Stability criteria are firmly established, it is capable of handling complex systems, and has the best accuracy of the finite differences methods [5].

Governing Equations

The governing equations for pipe flow, first presented in section 2.3, are repeated below for the readers convenience.

$$H_t + \frac{a^2}{g} V_x = 0 \tag{4.1}$$

$$gH_t + V_t + h_f = 0 \tag{4.2}$$

H is the piezometric head, the subscripts $_x$ and $_t$ denotes the spatial and temporal partial derivative respectively, g is the gravitational constant, V is the bulk flow velocity, h_f is the head loss per unit length and a is the wave propagation speed.

4.1 MOC - Quasi-Steady Friction

A commonly used representation of the MOC is the quasi-steady model. The head loss term, h_f is modelled by using the Darcy-Weisbach friction factor f. How to implement the MOC, as presented in [5], is described in this section.

$$h_f = f\frac{V|V|}{2gD} \tag{4.3}$$

D is the internal pipe diameter in the above equation. This representation of the head loss is computed in terms of the steady state conditions for a given velocity. The head loss will be updated as the velocities in the pipe change, hence the name, quasi-steady friction model.

4.1.1 Characteristics Equations

The continuity and momentum equations (4.1) and (4.2) form a pair of quasi-linear hyperbolic partial differential equations in terms of two dependent variables, velocity and hydraulic-grade-line elevation, and two independent variables, distance along the pipe and time. Skipping a few steps, the equations are formed into four ordinary differential equations by the characteristics method [5].

$$\left.\begin{aligned} &+\tfrac{g}{a}\tfrac{dH}{dt} + \tfrac{dV}{dt} + \tfrac{fV|V|}{2D} = 0 \\ &\tfrac{dx}{dt} = +a \end{aligned}\right\} C^+$$
$$\left.\begin{aligned} &-\tfrac{g}{a}\tfrac{dH}{dt} + \tfrac{dV}{dt} + \tfrac{fV|V|}{2D} = 0 \\ &\tfrac{dx}{dt} = -a \end{aligned}\right\} C^- \tag{4.4}$$

Equations (4.4) shows the change in position of a wave with related to the wave propagation velocity $dx/dt = \pm a$

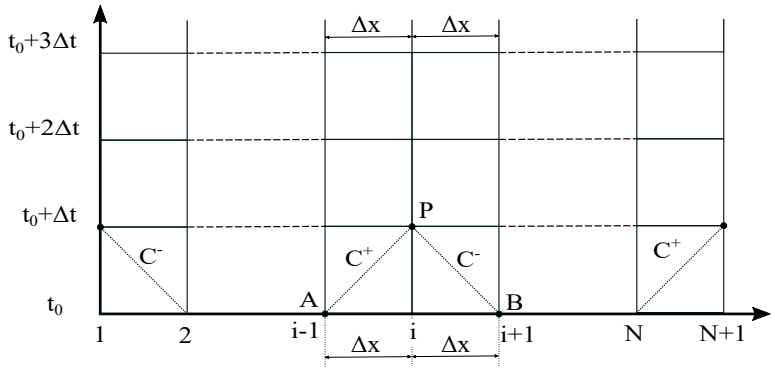

Figure 4.1: The characteristic lines in the xt plane

The ordinary differential equations (4.4) are valid along the characteristic lines C^+ and C^-. This impose the need of initial values as $x = ct - x_0$, for getting a solution for the domain. A solution can be found using the finite-differences equations.

The equations can be integrated along the characteristics leading to the following equations, the pipeline area is also introduced.

$$H_P - H_A + \frac{a}{gA}(Q_P - Q_A) + \frac{f\Delta x}{2gDA^2}Q_A|Q_A| = 0 \tag{4.5}$$

$$H_P - H_B - \frac{a}{gA}(Q_P - Q_B) + \frac{f\Delta x}{2gDA^2}Q_B|Q_B| = 0 \tag{4.6}$$

These two compatibility equations are basic algebraic relations that describe the transient propagation of pressure head and flow in a pipeline. Solving for H_P the equations can be written

$$C^+ : H_P = H_A - B(Q_P - Q_A) - RQ_A|Q_A| \tag{4.7}$$

$$C^- : H_P = H_B + B(Q_P - Q_B) + RQ_B|Q_B| \tag{4.8}$$

In which $B = a/(gA)$ and $R = f\Delta x/(2gDA^2)$.

These equations must hold for steady flow where $Q_A = Q_P = Q_B$ and $RQ_A|Q_A|$ is the steady-state friction term. If an exponential friction formula is preferred the last term of (4.7) can be changed to $R'Q_A|Q_A|^{n-1}$

The solution to a transient problem usually begins with steady-state conditions at time zero, so that H and Q are known initial values. Then H and Q are found for each grid point where $t = \Delta t$, then $t = 2\Delta t$ and so on. At any interior grid intersection point, section *i*, the two compatibility equations are solved simultaneously for Q_{P_i} and H_{P_i}. Equations (4.7) and (4.8) may be written in a simple form,

$$C^+ : H_{P_i} = C_P - BQ_{P_i} \tag{4.9}$$

$$C^- : H_{P_i} = C_M + BQ_{P_i} \tag{4.10}$$

in which C_P and C_M are always known from the variables of the previous time step.

$$C_P = H_{i-1} + BQ_{i-1} - RQ_{i-1}|Q_{i-1}| \tag{4.11}$$

$$C_M = H_{i+1} - BQ_{i+1} + RQ_{i+1}|Q_{i+1}| \tag{4.12}$$

Q_{P_i} can be eliminated from (4.9) and (4.10) which leads to the following:

$$H_{P_i} = (C_P + C_M)/2 \tag{4.13}$$

When H_{P_i} have been determined, then Q_{P_i} can be determined from either (4.9) or (4.10).

Examination of the grid in Figure 4.1 shows that the end points of the system begin influencing the interior points after the first time step. As previously mentioned, this method is dependent on knowing all values at a present time step before it can compute the next. Thus, it is necessary to introduce appropriate boundary and initial conditions.

4.1.2 Boundary and Initial Conditions

The end points of the system begin influencing the interior points after the first time step. As previously mentioned, this method is dependent on knowing all values at a present time step before it can compute the next. Thus, it is necessary to introduce appropriate boundary and initial conditions.

At the endpoints of a pipe, only one of the compatibility equations are known. At the upstream end, equation (4.10) holds, and at the downstream end, equation (4.9) holds. Hence an auxiliary function that specifies H_P, Q_P, or a relation between them, is required.

Upstream Boundary

An upstream reservoir keeping a constant head is described simply by equation (4.14). There will be minor variations, but it is usually okay to assume this to be constant. In [5], it is also described how to model minor changes in the reservoir.

$$H_{P_1} = H_R \tag{4.14}$$

Downstream Boundary

The flow through a closing valve can be modelled in different ways. It can be modelled to go to zero linearly, or by various other equations. Wylie and Streeter described the following general equation which is applicable for a closing valve downstream [5].

$$Q_P = \frac{Q_0}{\sqrt{H_0}} \tau \sqrt{\Delta H} \tag{4.15}$$

The dimensionless valve opening, τ is defined so that $\tau = 1$ for steady flow and $\tau = 0$ for a closed valve. A system with closing time t_c, can be simulated with the equation $\tau = (1 - \frac{t}{t_c})^{E_m}$. A sinusoidal boundary can also be implemented be changing τ to a sinusoidal function.

Solving equations (4.9) and (4.15) simultaneously gives the following relation.

$$Q_{P_{NS}} = -BC_v + \sqrt{(BC_v)^2 + 2C_vC_P} \tag{4.16}$$

The subscript NS is appended to the variables Q_P and H_P such that $Q_{P_{NS}}$ denotes the last element of the pipe, adjacent to the outlet boundary. C_v is defined so that $C_v = (Q_0\tau)^2/(2H_0)$.

4.1.3 Complex systems

For the sake of this work, a single pipe system will be considered. However, for more complicated systems, such as bifurcations and change in pipe diameter, Wylie and Streeter [5] provides methods that are relatively easy to implement. As they could hold relevance to possible future work, they are added to Appendix B.

4.2 Stability and Alternating Wave Speed

A stability criterion for solving partial differential equations numerically is given by the Courant-Friedrichs-Lewy (CFL) condition [32]. The condition creates a dependency between the temporal and the spatial step with the Courant number C_r. For the MOC, the relation is $C_r = a\frac{\Delta t}{\Delta x}$. Keeping the Courant number, as close to unity as possible virtually means having the characteristic lines crossing the time-lines as close to a computational node as possible. The closer to a node the lines intersect, the smaller the numerical error will be. Hence having small time step, and small Δx will minimize the error from the numerical computation. Normally for the MOC, the time step is decided for $C_r = 1$. For the stability criterion the Courant number cannot exceed one. A numerical scheme with a Courant number larger than one does not converge.

The CFL condition additionally implies that there is no extrapolation of values. All the values used in the numerical scheme must be found through interpolation [33].

When there is a complex system with alternating wave speed, the slope of the characteristic line may vary, meaning that the intersection point of the lines will not be exactly at point P of the grid. This introduces the need to interpolate in order to find nodal point values. Interpolation will introduce some added numerical error, and the size of the error will depend on how fine the grid is.

4.3 MOC - MIAB Friction

The method for solving the governing equations, Equation 4.1 and Equation 4.2, using MOC with MIAB friction model is very similar to the quasi-steady friction model. The differences spawn from the head loss term, h_f. The MIAB head loss term, presented in section 3.4, is repeated here.

$$h_{f,u} = \left(\frac{k_t}{g} \frac{\partial V}{\partial t} + \frac{k_x a \phi}{g} \frac{\partial V}{\partial x} \right) \tag{4.17}$$

In the following section, the derivation of MOC with the MIAB friction model is briefly presented. For a more thorough derivation, see Appendix A.

4.3.1 Characteristics Equations with MIAB Friction Model

The derivation of the characteristics equations for MIAB model is slightly different than the quasi steady model as the friction term is different. Using a similar procedure, the characteristic equations are obtained.

$$\begin{aligned} &\left.\begin{aligned} &\lambda \tfrac{dH}{dt} + (1+k_t)\tfrac{dV}{dt} + \tfrac{fV|V|}{2D} = 0 \\ &\tfrac{dx}{dt} = \tfrac{2a}{-\phi k_x + \sqrt{k_x^2 + 4(1+k_t)}} \end{aligned}\right\} C^+ \\ &\left.\begin{aligned} &\lambda \tfrac{dH}{dt} + (1+k_t)\tfrac{dV}{dt} + \tfrac{fV|V|}{2D} = 0 \\ &\tfrac{dx}{dt} = \tfrac{-2a}{\phi k_x + \sqrt{k_x^2 + 4(1+k_t)}} \end{aligned}\right\} C^- \end{aligned} \tag{4.18}$$

$$\begin{aligned} C^+ \quad &\Rightarrow \quad \lambda = \frac{-\phi k_x + \sqrt{k_x^2 + 4(1+k_t)}}{2a/g} \\ C^- \quad &\Rightarrow \quad \lambda = \frac{-\phi k_x - \sqrt{k_x^2 + 4(1+k_t)}}{2a/g} \end{aligned}$$

A notable difference between this method, and MOC with a QS friction model, is the difference in the inclination of the characteristic lines, dx/dt. Not accounting for transient friction, the characteristic lines would be given solemnly by the wave speed, $dx/dt = \pm a$. However the transient friction provides the slightly more complicated characteristic lines seen in Equation 4.18.

The ordinary differential equations (4.18) are valid along the characteristic lines C^+ and C^-. This impose the need of initial values as $x = ct - x_0$, for getting a solution for the domain. A solution can be found using the finite-differences equations. The derivation of the discretization is presented in Appendix A. Here the equations that are to be solved by the program are presented.

$$C^+ : H_{P_i} = C_P - B^+ Q_{P_i} \tag{4.19}$$

$$C^- : H_{P_i} = C_M + B^- Q_{P_i} \tag{4.20}$$

As B^+ and B^- are introduced with different values, one cannot solve the equation the same way as in the quasi-steady solution. Instead, H_{P_i} can be eliminated from (4.19) and (4.20) which leads to the below equation.

$$Q_{P_i} = \frac{C_P - C_M}{B^- + B^+} \tag{4.21}$$

When Q_{P_i} have been determined, then H_{P_i} can be determined from either (4.19) or (4.20).

The way the loss is modeled in the MIAB model causes the inclination of C^+ and C^- to change. Figure 4.2 shows how the characteristic lines deviate when transient friction is accounted for.

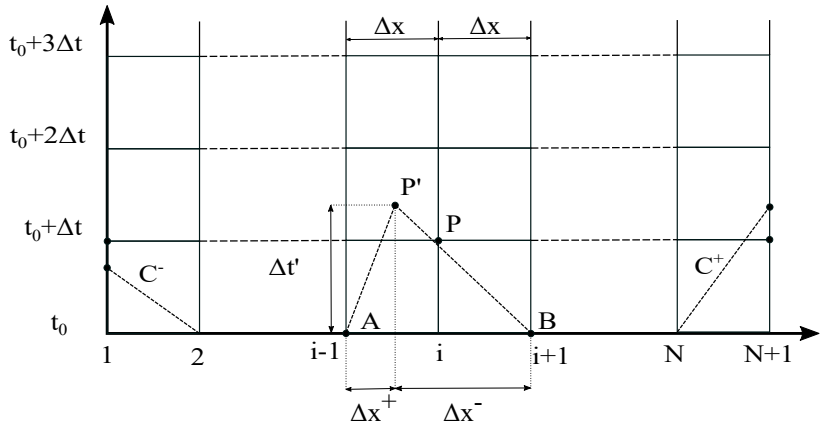

Figure 4.2: The grid used with MOC and MIAB friction model

In a MOC model with a steady state friction model, all the characteristic lines have the same inclination. The grid is then modified so that the lines hit the same point P for the same Δt. In the MIAB model however, this is not the case, and Δt will vary and the Q_{P_i} and H_{P_i} computed from the characteristic lines does not align perfectly with the grid. A solution to this problem is interpolation, however, this may impose some numerical error on the model.

The full interpolation scheme is covered in detail in Appendix A. Interpolating affects the efficiency as well as the added numerical error. However, it is still a fast and accurate scheme.

4.4 MOC- Zielke's Friction

The implementation of the friction model first introduced by Zielke and presented in chapter 3 is described subsequently.

Equation 4.2 and Equation 4.1 are solved with Equation 3.5. The head loss term is repeated here.

$$h_f = h_s + 16\frac{\nu}{gD^2}\int_0^t \frac{\partial V}{\partial u} W_0(t-u)du \tag{4.22}$$

In which h_f is the new friction term to be used with Equation 4.2, h_s is the quasi-steady component usually computed using Darcy-Weisbach friction formula and ν is the kinematic viscosity.

The weighting function given as $W(\tau)$ where $\tau = 4\nu t/D^2$, has been subjected to numerous changes. A large variety is presented and assessed by Vítkovskỳ et al. (2004). The one chosen for this model was developed for laminar and turbulent flow in smooth pipe by Vardy and Brown.

$$W(\tau) = \frac{A^* e^{-B^*\tau}}{\sqrt{\tau}} \tag{4.23}$$

For laminar flow $B^* = 210.08$ and $A^* = 1/(2\sqrt{\pi})$. The intended use for this model is a simulation with a Reynolds number of 1870, which is well within the laminar regime. For a turbulent case, A^* and B^* are computed from the viscosity and the Reynolds number.

The numerical implementation is done according to Equation 4.24. In the summation, j denotes the spatial variable, and k is the temporal variable. As seen from the equation, Zielke utilizes all velocities from all previous time steps. For large simulations with small time step and grid, the memory required and computational time will be very large. For a small and short simulation, however, it is efficient and precise.

$$h_u^i(k\Delta t) = 16\frac{\nu}{gD^2}\sum_{j=1,2..}^{k-1}(V_j^i - V_{j-1}^i) * W[(k-j)\Delta t] \tag{4.24}$$

The head loss term is easily implemented with the MOC. Even though the implementation is uncomplicated, the method quickly becomes time consuming as simulation time increases. This is because the method computes the friction from all previous velocities in every time step. But for small simulations it is a relatively fast and reliable method.

Chapter 5

Concerning Coupling

5.1 1D Model

The 1D model, mathematically described by the Allievi's equations presented in section 2.3, is based on assumptions related to the 1D nature of the pipe flow. It was developed for efficient and accurate simulation of transient phenomena occurring in the water conveying systems with a simple geometry. The 1D MOC has been widely used an validated since the 50's [5].

This paper focuses on the friction model of the 1D MOC, which has been thoroughly presented in chapter 3. In addition, there is the question of the 1D nature of the flow variables in this method, and how they translate to 3D. section 5.2 presents a literature study on various coupling methods.

Using the pressure gradient from the MOC, a 2D velocity profile can be generated, and possibly be used as an intermediate step between 1D and 3D model. The process will be described in detail in section 5.3.

3D Model

The 3D CFD model is not utilized for the work in this thesis. Nonetheless, a literature study on how to model compressibility in water was conducted. In addition model order reduction was briefly researched. The interested reader can find information on this in Appendix C.

5.2 Coupling Methods

The fundamental idea for a coupled model is to divide the computational domain into different regions. The 3D CFD model will be applied in the sections where streamlines change rapidly over a short distance, for example in a turbine. In the pipelines, the flow variables change almost only along the central streamline, and can be simulated by a 1D model, such as the MOC.

The data exchange between the 1D and 3D model is of utmost importance when connecting the models. For the sake of coupling, numerous different methods are described in the literature [34, 35, 36, 37, 38, 39], with applications in the biological world as well as in hydropower. As different numerical methods have different stability criteria, time steps may differ between schemes presenting the need for iterative coupling methods. Iterative coupling methods will however provide an additional inaccuracy to the simulation. Hence, the non-iterative methods are of greater interest.

Wang et al. [40] used a non-iterative method based on Riemann-invariants giving an accurate and robust 1D-3D coupled model. The model accurately captures and transmits the pressure surge at the boundary between 1D and 3D. The authors also assess the importance of the placement of the 1D-3D boundary. Ideally the 3D domain is limited in order to save computational time. However, if the 1D-3D interface is too close to a region with 3D effects, the flow at the interface may not be 1D and could possibly affect the coupling. Wang recommends that the distance between the coupling interface and the geometrically non-1D region is not less than 5 times the cross-sectional dimension at the interface.

Wu et al. [41] set up a MOC-CFD coupled model for analyzing the fluid dynamic interaction between water hammer and pump. Fluent code was used for the 3D CFD model. The coupled model was compared to using MOC calculations alone. The transient simulation demonstrated that the 1D-3D coupled analysis was closer to real conditions because it considers the effect of fluid inertia. This is suggesting that 1D-3D coupling can be a good option for simulating fluid transients in the penstock.

Zhang and Cheng [39] presented two models, namely, the Partly Overlapped Coupled method (POC), and the Adjacent Coupling method (AC). For the AC method, the grids are adjacent as depicted in Figure 5.1 (a). The goal is to compute the piezometric head, H_P^{n+1}, and flow rate, Q_P^{n+1}, of cell P^{n+1}. This could be done by using for example the unsteady Bernoulli equation. This method makes sense physically, however, the method is more complicated than the POC.

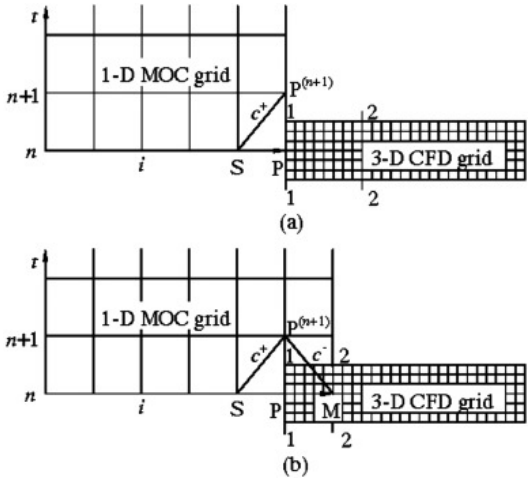

Figure 5.1: Illustration of **(a)** Adjacent Coupling (AC) and **(b)** Partly Overlapped Coupling (POC) taken from [39]

The POC is illustrated in Figure 5.1 (b). For this method, the node P is no longer the downstream boundary. Thus, another characteristic line, C^-, can be constructed and the characteristic equations can be solved for the cell P^{n+1}.

$$C^- : H_P^{n+1} = H_M^{(n)} + B\left[Q_P^{(n+1)} - Q_M^{(n)}\right] \tag{5.1}$$

In Equation 5.1, Q_M and H_M are located inside the CFD domain, hence the name. To use the values from the CFD to construct the characteristic line C^-, the section average flow rate and head has to be computed. After finding $Q_P^{(n+1)}$ and $H_P^{(n+1)}$, they are designated as boundary conditions for the CFD simulation. Note that these methods are non-iterative, implying that the solution from both schemes needs to be known at a given time and numerical errors may cause spurious transients.

The conclusion of the 2012 study by Zhang and Cheng [39], is that both the methods are valid and accurate. The POC requires more computational resources from the CFD, however it is easier to implemented. In a newer study by Zhang et al. [42], the authors stated that the POC holds superior efficiency and accuracy. It is safe to say that the method is promising, and should be the subject of further studies and investigation.

5.3 1D to 2D; the Heat Equation

The 1D models use variables that are averaged over a cross section, while the velocity and pressure will vary over the added dimensions in a 3D model. How the variables are communicated between a coupled model is essential to the performance. An interesting method, primarily suggested by Storli[1], is reducing the Navier-Stokes(NS) equations until it has the same form as the parabolic heat equation. The heat generation term, q, of the heat equation can be replaced by the pressure gradient from the NS equation. Solving the new differential equation will provide a velocity profile. The mathematical procedure is presented below.

The heat equation in cylindrical coordinates,

$$\frac{\partial u}{\partial t} = c^2\left(\frac{\partial^2 u}{\partial r^2} + \frac{1}{r}\frac{\partial u}{\partial r} + \frac{1}{r^2}\frac{\partial^2 u}{\partial \theta^2} + \frac{\partial^2 u}{\partial z^2}\right) + q \tag{5.2}$$

The z-component of NS in cylindrical coordinates,

$$\begin{aligned} \rho\left(\frac{\partial u_z}{\partial t} + u_r\frac{\partial u_z}{\partial r} + \frac{u_\theta}{r}\frac{\partial u_z}{\partial \theta} + u_z\frac{\partial u_z}{\partial z}\right) = \\ -\frac{\partial p}{\partial z} + \mu\left[\frac{1}{r}\frac{\partial}{\partial r}\left(r\frac{\partial u_z}{\partial r}\right) + \frac{1}{r^2}\frac{\partial^2 u_z}{\partial \theta^2} + \frac{\partial^2 u_z}{\partial z^2}\right] + \rho g_z \end{aligned} \tag{5.3}$$

In this equation the different subscripts for u denotes the velocity in the z, r or θ direction. The z-component of NS is reduced based on laminar flow assumptions. The simplification of the equations only contains the velocity, u_z. Hereby u will be used to denote the velocity in the z-direction.

[1] This method is not documented in the literature. Storli used the technique in a presentation at the 24th IAHR Symposiom in Brazil 2008. The presentation was related to a publication by Storli and Nielsen [3].

Reduced form of NS:

$$\frac{\partial u}{\partial t} = \frac{\mu}{\rho}\left(\frac{\partial^2 u}{\partial r^2} + \frac{1}{r}\frac{\partial u}{\partial r} + \frac{\partial^2 u}{\partial z^2}\right) - \frac{1}{\rho}\frac{\partial p}{\partial z} \tag{5.4}$$

Reducing the heat equation similarly provides the following equation.

$$\frac{\partial u}{\partial t} = c^2\left(\frac{\partial^2 u}{\partial r^2} + \frac{1}{r}\frac{\partial u}{\partial r} + \frac{\partial^2 u}{\partial z^2}\right) + q \tag{5.5}$$

From the 1D solvers, the time history of the pressure and velocity can be obtained. With this information, the reduced NS can be solved to produce a velocity profile. The reduced NS equation can be solved in the same way as the parabolic heat equation.

Many commercial and non-commercial software provides a built in solver for the heat equation. For this work, MATLAB's solver, **pdepe**, will be used and the solver requires the equation to be on the following form.

$$c\frac{\partial u}{\partial t} = x^{-m}\frac{\partial}{\partial x}\left(x^m f(x,t,u,\frac{\partial u}{\partial x})\right) + S \tag{5.6}$$

In order to match the input required, the NS is modified in the following manner.

$$\frac{1}{\nu}\frac{\partial u}{\partial t} = \frac{1}{r}\frac{\partial}{\partial r}\left(r\frac{\partial u}{\partial r}\right) + \left(\frac{\partial^2 u}{\partial z^2} - \frac{1}{\mu}\frac{\partial p}{\partial z}\right) \tag{5.7}$$

Solving these equations numerically will provide a velocity profile.

Note that the reduction of the NS equation is based on laminar pipe flow. Using this method to produce a velocity profile for turbulent pipe flow would produce wrongful results. A time averaged turbulent velocity could possibly be approximated by modifying the viscosity, similar to the principles of eddy viscosity. This is the basis of the simulations presented in subsection 6.3.1 and section 7.3.

Chapter 6

Simulation Set Up

For the sake of validating the 1D models, and the friction models, the results from the models have been compared to an experiment performed by Bergant et al. [2]. The experiment was conducted to investigate unsteady friction in 1D models, and it will be used to validate the 1D models in this work.

6.1 Physical Set Up

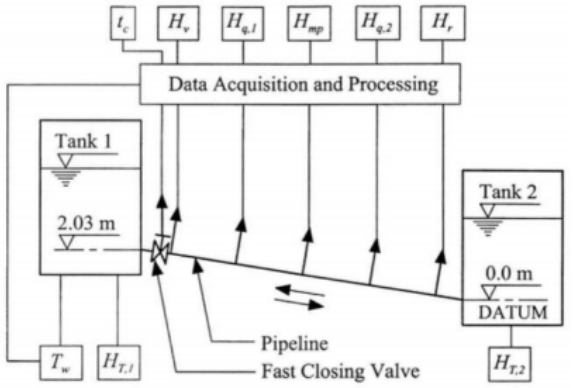

Figure 6.1: Illustration of Bergant's experiment, taken from [2]

Bergant's experimental rig consists of two tanks connected by a thin pipe of diameter, D, and length, L. The tanks are pressurized, and regulated to keep a constant head. This makes it possible to modify the reservoir pressure denoted H_r. The wave propagation speed, a, was analytically computed by Bergant et al. [2]. t_c denotes the closing time of

the downstream valve and t is the full time of the recording. Re is the Reynolds number. The properties related to the experiment is listed below.

- $L = 37.23\,m$
- $D = 2.21\,cm$
- $H_r = 32\,m$
- $V_0 = 0.1\,m/s$
- $a = 1319\,m/s$
- $t_c = 0.009\,s$
- $t = 1.5\,s$
- $Re = 1870$

6.2 1D Simulation

Implementation of the 1D methods is described in detail in chapter 4. There are certain properties that are vested to certain friction models, and those will be presented in this section.

All of the models were coded in MATLAB R2020a. The full code of the various friction models are added to Appendix D.

For all the 1D simulations, the pipe was divided in N reaches, resulting in $N + 1$ grid points. Following properties were the same for all the friction models: the gravitational acceleration, g, the Darcy-Weisbach friction factor, f and the density, ρ_0. Note the density ρ_0 is the density for water at $15.5°$C. The values corresponding to the variables are listed below.

- $N = 1001$
- $g = 9.8066502\,m/s^2$
- $f = 0.0345$
- $\rho_0 = 999.057$

6.2.1 Quasi-Steady Friction Model

No further info needed to model this one

6.2.2 MIAB Friction Model

This method introduces several new computational steps, as it requires an interpolation scheme, however it only introduces two new variables as compared to the quasi-steady model. The friction model is based of spatial and temporal derivatives of the velocity, which requires one factor for each derivative. k_t represents the temporal factor and k_x the spatial factor. Their values are listed below. Their values were found through trial and error. The starting point, was the analytically determined value of 0.0345 from Bergant et al. [2].

- $k_t = 0.04$
- $k_x = 0.03$

6.2.3 Zielke's Friction Model

The main difference between Zielke's and the other friction models is that Zielke's model stores all the velocities of the previous times. This is because the friction model uses velocities of previous time steps to compute the head loss term, h_f, as presented in section 4.4. In addition, the model needs the parameters for the viscosity, ν, and the variables, $A*$ and $B*$, for the weighting function, W. The viscosity ν is computed from the Reynold's number given by Bergant et al. [2]. The values of $A*$ and $B*$ are the values for laminar flow as presented in [23].

- $\nu = 1.1818...e-06$
- $A* = 1/(2\sqrt{\pi})$
- $B* = 210.08$

6.3 Heat Equation

Matlab will be used to solve the parabolic partial differential equation, which is a simplified version of NS momentum equation. **pdepe**, a pre-programmed solver in MATLAB, is used to obtain a solution. The method for using this solver is briefly described in this section, and the full script will be added to Appendix E. As stated in section 5.3, the NS momentum equation is modified so it is on the following form.

$$\frac{\partial u}{\partial t} = c\left(\frac{\partial^2 u}{\partial r^2} + \frac{1}{r}\frac{\partial u}{\partial r} + \frac{\partial^2 u}{\partial z^2}\right) + S$$

The variables which are taken from the simplified version of NS momentum equation are listed here.

- $c = \frac{1}{\nu}$
- $x = r$
- $m = 1$
- $S = \frac{\partial^2 u}{\partial z^2} - \frac{1}{\mu}\frac{\partial p}{\partial z}$

The variable z denotes the lengthwise direction of the pipe, S is the source term and the spatial variable, x, will cover the radius of the pipe. In MATLAB, the PDE-solver is called upon by the following command.

sol=pdepe(m,pdefun,icfun,bcfun,xmesh,tspan)

- **m** is the symmetry constant, for cylindrical coordinates **m** $= 1$
- **pdefun** defines the equations being solved.
- **icfun** defines the initial conditions.

- **bcfun** defines the boundary conditions.
- **xmesh** is a vector of spatial values for x, it represents the pipe diameter.
- **tspan** is a vector of the time values for the variable, t

This setup allows the user to define the equation to be solved, the boundary conditions, initial conditions, as well as the grid on which it will be solved. For the pipe wall, a no-slip condition was imposed, and the pressure gradient was used as a source term in the equations.

Steady State

First the model was tested for a steady state case, in which the source term, S is constant, and can be computed from the Darcy-Weisbach formula. The Darcy-Weisbach friction factor was introduced for the 1D quasi steady MOC, and has the value, $f = 0.0345$. In addition, the model needs information on the viscosity, the value for which was already introduced for Zielke's friction model, $\nu = 1.1818... \times 10^{-6}$. At last, the density is $\rho = 999.057$.

Unsteady Simulation

For the unsteady mode, the main change is the source term. This is no longer constant, instead it is $S = u_{zz} - \frac{1}{\mu}p_z$. All these values can be taken from any of the 1D models. For the sake of comparing, simulations using data from all three friction models have been conducted. The no-slip condition at the wall is still in effect. However, the **tspan**-vector has to be adapted to fit with the variables taken from the MOC models. This is done simply by using the same time step as in the MOC.

6.3.1 Turbulent Flow

Solving a reduced version of Navier-Stokes equation is an interesting way of generating a 2D velocity profile. Nonetheless, it holds little relevance to research related to hydro power machinery, unless, it is applicable for turbulent flow. When reducing the NS equations, as in section 5.3, there is only considered to be a velocity in the lengthwise direction of the pipe. Turbulence, however, also implies radial motion. Solving the parabolic differential equation from NS will not solve for this motion. However, using a modified viscosity, as presented in section 2.6, the time-averaged velocity in the lengthwise direction can be estimated.

For this test simulation, a diameter, D, and Reynolds number were chosen at random. Viscosity and density was chosen water at 20°C. Flow properties are summed up below.

- $Re = 7000000$
- $f = 0.011$
- $\rho = 998.2 kg/m^3$
- $\mu = 1.002 * 10^{-3} Pa/s$

- $\bar{u} = 14.0602 m/s$, computed from Re, μ, ρ and D

Using the information above, combined with the Darcy-Weisbach head loss formula, provides the necessary information to compute a pressure gradient for a steady state case. However, solving the partial differential equation with a constant viscosity will return a laminar profile with a flow rate several orders of magnitude greater than the actual flow rate. This problem was solved by empirically creating a position dependent viscosity. Using symmetry around the centerline in the pipe, the viscosity was set to only vary along the radius, r. The reverse S-shaped function with the following mathematical representation was utilized for this purpose.

$$\nu(r) = \frac{C_1}{1 + \exp C_2 r - C_3} - C_4 r \tag{6.1}$$

C_1, C_2 and C_3 are constants which needs to be determined empirically. Thus the simulation will be run several times, while changing the constants. The original flow rate and the power law velocity profile will provide useful comparison when determining the coefficients.

Chapter 7

Results & Discussion

Bergant's water hammer experiment [2] is used as base for the simulation. The details of this experiment can be found in chapter 6. The first part of this chapter, section 7.1, will compare the results from the 1D simulations to the results reported by Bergant et al. [2]. The heat equation is tested and discussed in section 7.2, and section 7.3 applies the heat equation to steady state turbulent velocity conditions. In section 7.4, coupling of 1D and 3D models is discussed on the basis of the presented literature and work and possible further work is considered

7.1 1D MOC Simulations

The 1D models were presented in chapter 4, and the specific properties used for this experimental set up were presented in section 6.2. In the 1D models, the water hammer was actualized by letting the discharge, at the downstream outlet, go to zero over a closing time t_c. Comparing the results to Bergant's experiment [2] will provide information on the models performance. In addition, the simulations can be compared and validated against previous simulations. The main parameters to observe for the 1D models will be the following.

- **Attenuation of the pressure head**.
  The frictionless MOC is known not to be able to approximate the wave attenuation correctly. Capturing the attenuation correctly is crucial for the friction model.

- **Phase shift**
  The phase of the transient pressure is also heavily impacted by the choice of friction model, and will be assessed.

- **Computational time**
  The computational time from the various models will be presented. It is not the main focus in this thesis, however, it should be kept in the back of the mind.

The location from which data is observed and compared is the node adjacent to the closed valve. For the 1D models consisting of N reaches and $N + 1$ nodes, it will be node number $N + 1$, counting from the upstream inlet.

7.1.1 Quasi-Steady Model

Transient pressure head for the quasi-steady model, compared to Bergant's experimental results, is depicted in Figure 7.1. MOC with a quasi-steady friction model aligns well with the experimental results for the two first rises in the pressure. After which, the models show insufficient attenuation of the pressure head. Around $0.5s$ the phase shift becomes clearly visible. Approaching $1.5s$, the simulation fails to model both phase shift, and the attenuation of the pressure head.

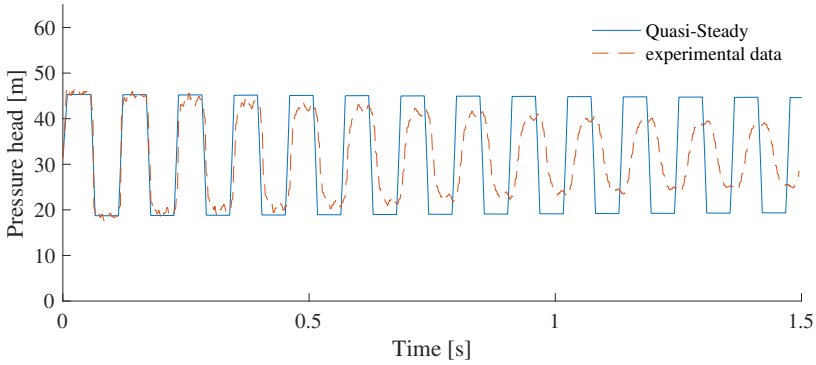

Figure 7.1: MOC with Quasi-Steady friction model vs experimental results from [2]

As expected, the QS friction model fails to accurately attenuate the pressure amplitudes, it also fails in modelling the phase shift. This is the same as the results of Bergant et al. [2]. The QS model does not account for the effects of transient friction, and, as stated in the beginning of chapter 3, transient friction has to be accounted for in small pipes with flow of a low Reynold's number.

7.1.2 MIAB Model

Figure 7.2 shows the transient pressure for the MOC with a MIAB friction model and the experimental results. For this model, the coefficients, k_t and k_x, were based on the analytical value found by Bergant et al. [2] for this set up. The coefficients were then altered slightly to become the values presented in subsection 6.2.2. This model is able to capture both the attenuation and phase shift. Out of the three friction models considered for the given case, the MIAB model shows the best fit with the experimental results.

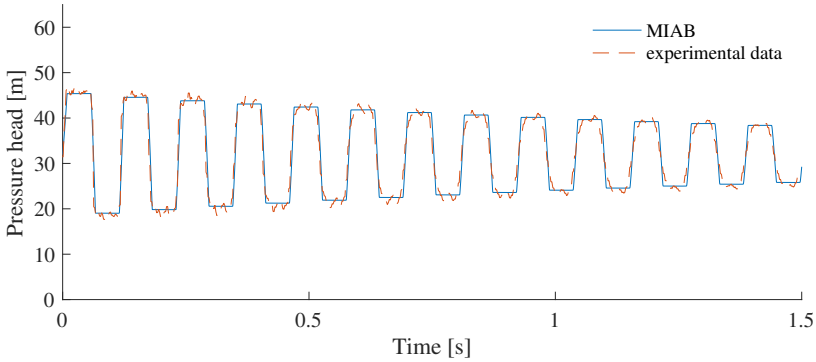

Figure 7.2: MOC with MIAB friction model vs experimental results from [2]

The MIAB model shows the best fit among the three friction models. This is also in accordance with Bergant et al.'s results, who used a model referred to as *Brunone's model*. Brunone's model, is an IAB model with one friction coefficient, whereas Figure 7.2 shows the transient pressure for a MIAB model with two friction coefficients. The results are very similar, and the best fit of all three friction models tested for this specific case.

7.1.3 Zielke's Model

Figure 7.3 shows MOC were the head loss term is modelled with Zielke's friction model. Compared to the experiment, this model shows discrepancy with both the phase shift, and attenuation of the pressure head. The results are still close to the experimental data, but the MIAB model clearly shows better match. In previous studies, similar results have been found for the models [2, 10]. The computational time required for this model is quite extensive as it takes in all the previous time steps when computing the head loss term.

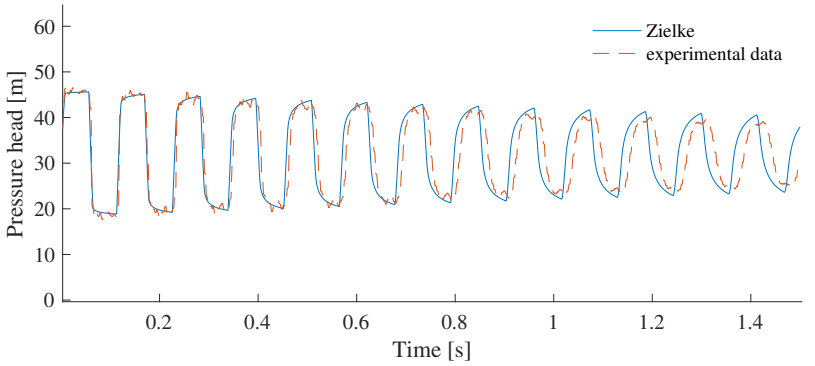

Figure 7.3: MOC with Zielke's friction model vs experimental results from [2]

Zielke's model show much better fit with experimental results than the QS model.

However, it is not matching with experimental results as well as the MIAB model. Note that the CPU time of Zielke's simulation is approximately 4500 times more than that of the QS model and 350 times that of the MIAB model.

Model	CPU-time $[s]$
QS	1.25
MIAB	16.5
Zielke	5673

Table 7.1: Seconds CPU-time of the different friction models used with the MOC

Efficient simulations are crucial, and although the simulation time for this specific experiment is low, it will quickly rise for larger systems such as hydro power stations. The CPU time used by the MIAB model is approximately 350 times less then that of Zielke's model, and the QS model is around 4500 times less than Zielke's. In addition, Zielke's model becomes slower and requires more memory the longer a simulation runs for. In its full state the model would quickly become too slow and consume too much memory for practical use. However, its efficiency can be improved by only using the most recent time steps and not all time steps since the beginning of the simulation. The most recent accelerations have the largest impact on the solution thanks to the weighting function. After a certain time, the contribution of previous velocity changes will become negligible, and can be dropped without loosing significant accuracy in the solution. This could save large amounts of both CPU time and memory use. Although Zielke's model is made more efficient, it is less likely to become faster than the MIAB. It may still be a preferred option as it does not have coefficients that need to be predetermined, as does the MIAB. The modified Zielke's model is an interesting option, and should be investigated further.

Once again, the experimental set up used for the various 1D models is taken from Bergant et al. (2001). Additionally, simulations of the friction models applied in the previous section has already been documented for this specific set up the literature [2, 10]. These results serve to validate the 1D models used for the work in this thesis.

The transient pressure plots of the different friction models are all validated when tested.

7.1.4 Discussion; 1D friction models

The purpose of a 1D-3D coupled simulation is to study the interaction between the runner and the waterway. Pressure pulses are generated at the runner, and will then propagate in the waterway. It is important that the simulation is able to conserve the correct pressure amplitudes and frequencies. The coupled model cannot be more accurate than its 1D and 3D components, and so it is crucial that the 1D model simulates the pressure pulse accurately.

For the experimental set up considered, it is apparent that a model accounting for transient friction is necessary, in order to achieve meaningful results. The different friction models affects both amplitude and phase of the pressure pulse. In the simulations, the frequencies and amplitudes of the pressure pulsations are of utmost importance, and it is

crucial to choose a friction model which is able to capture these flow features correctly. In terms of a 1D-3D coupled simulation, choosing the wrong friction model could lead to an erroneous altering of the pressure wave amplitude and frequency as it passes through the 1D model.

It is important to note that these tests are done for laminar flow. Turbulence will largely be present in actual hydro power stations, and as presented in section 7.3 the choice of friction model will change with an increasing Reynold's number. In essence, experiments with flow conditions closer to that of hydro power stations would certainly be recommended for testing the friction models, as not a lot of data is available in the literature.

For a hydro power station, a water hammer simulation is a type of worst case scenario simulation. An unsteady friction model may lead to underestimating the pressure peaks and thus the impact from the water hammer. Simulating a water hammer may not even be necessary, as it can easily be avoided by making sure the distance to the surge tank is small enough to completely avoid the severe transient. Fatigue loads for turbines in hydro power stations are usually related to normal operating conditions, accordingly, one would be interested in simulations related to normal operating conditions. It is important for the model to capture amplitudes and frequencies of the relevant pressure pulsations that occur under normal operating conditions, not necessarily model a water hammer to perfection. For pressure pulses of smaller amplitudes than a water hammer, the effect on the velocity profile and its gradient will not be as large, and the relevance of unsteady friction is likely to be less. It would be interesting to compare the different 1D friction models on how they simulate pressure pulses of smaller amplitudes and higher frequencies than the water hammer.

7.2 Heat Equation for a 2D Velocity Profile

Results from the reduced NS momentum equation is presented in this section. As presented in section 5.3, the momentum equation is reduced until it is on the same form as the heat equation. Then, the heat generating term is replaced by a pressure gradient taken from the 1D model. Firstly, a simulation was run with a constant pressure gradient, to obtain steady state conditions. After which, the transient pressure gradient from the 1D models was added to the numerical scheme.

7.2.1 Steady State Simulation

For the steady state simulation, the initial conditions for the velocity were zero. The scheme was then run until the velocity converged. Figure 7.4 shows the change of the center velocity versus simulation time. When the simulation time is at around $150s$, there appear to be little to no change in the velocity.

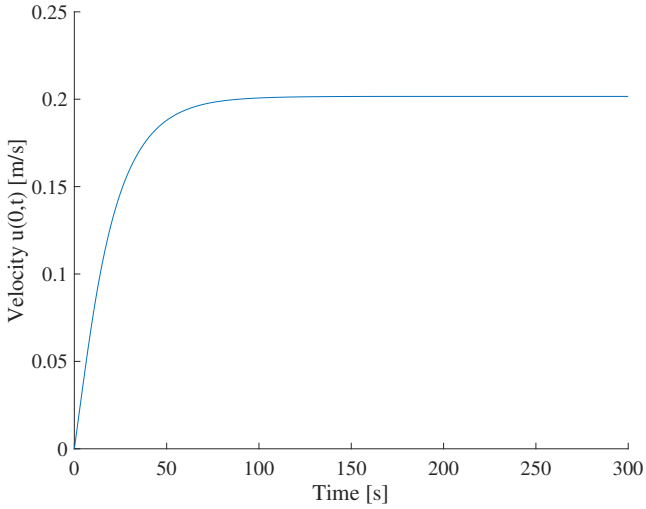

Figure 7.4: Convergence of center velocity

Figure 7.5, on the next page, shows the velocity profile produced from the steady state simulation. Essentially, this is the velocity profile for the fully developed flow throughout the pipe. The velocity profile has the form of a fully developed laminar profile, which is meaningful as the Reynolds number is 1870. Additionally, the flow rate of the new velocity profile is $Q = 3.8652 \times 10^{-5} m^3/s$, which is very close to the initial flow rate for the MOC of $Q = 3.8360 \times 10^{-5} m^3/s$.

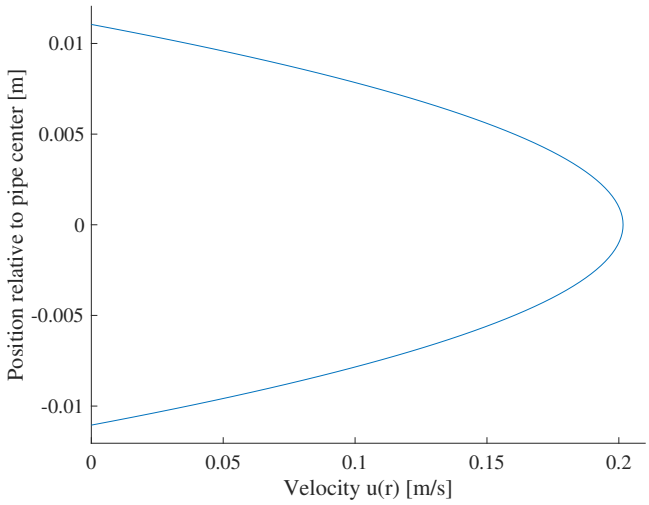

Figure 7.5: Velocity Profile

In terms of producing a velocity profile for the steady state case, the heat equation was successful. The flow rate was 1.0076 times the initial flow rate. The flow rate generated using the heat equation is affected by the choice of viscosity and density, in addition to the radial refinement. The flow deviates from the original flow rate by 0.76%. When compared to a theoretical velocity profile for laminar flow, the profile produced by the heat equation shows excellent fit.

Note that the error in flow rate is likely related to the viscosity. The viscosity was computed based on the Reynold's number of 1870, given by Bergant et al. [2].

7.2.2 Transient Simulation

The velocity profile presented in the previous section was used as initial conditions for the transient simulation. For this simulation, the time step and pressure gradient term were taken from the MOC simulation. With these conditions, the equations were solved in time numerically. The pressure gradient is taken from a location $7.44m$ from the inlet, or node number 200. The pipe is $37.23m$ from inlet to outlet and is divided into 1001 reaches. At this location there is great variations in the velocity profile, so it serves well as an illustration.

Figure 7.6 Shows what happens to the velocity profile when the first pressure rise arrives, and the average velocity becomes zero approximately at $t = 0.0282s$. Although the average velocity for the cross section is zero, there is still a velocity profile with both negative and positive velocities. Eventually, back flow occurs as a result of over pressure in the pipe, and the velocity becomes fully negative at $t = 0.0451s$. For the fully negative velocity profile, the largest velocity is observed close to the pipe wall, with large velocity gradients occurring near the wall.

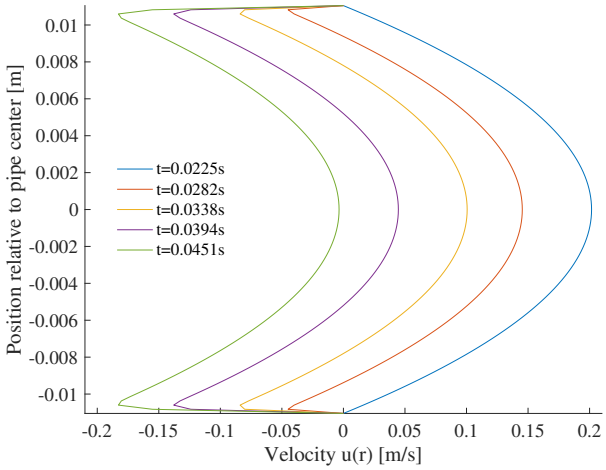

Figure 7.6: Transient velocity profile from $t = 0.0225s$ to $t = 0.0451s$

Figure 7.7 shows the velocity profile as the flow transitions from negative at $t = 0.0789s$ to positive at $t = 0.101s$. When the velocity returns to being positive, as it was initially, the shape of the velocity profile is changed. The shape in the middle is close to the same, however, there is another peak near the wall. Although it has a smaller velocity than the middle section, the velocity gradient near the wall is much steeper than in the initial velocity profile.

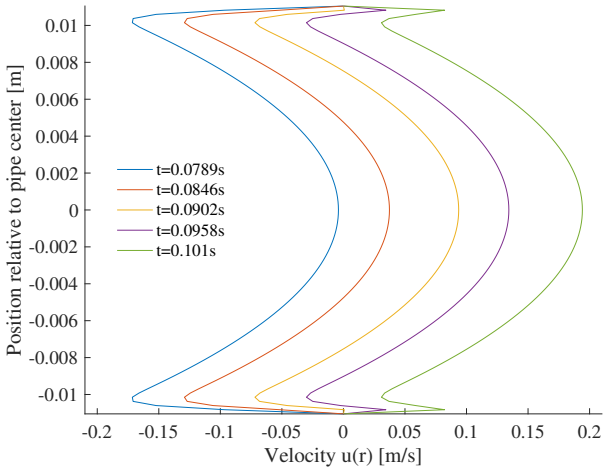

Figure 7.7: Transient velocity profile from $t = 0.0789s$ to $t = 0.101s$

Figure 7.6 and Figure 7.7 shows the velocity profile generated based on the gradient taken from node number 200 in the simulation. Figure 7.8 Shows the pressure related to

the same node.

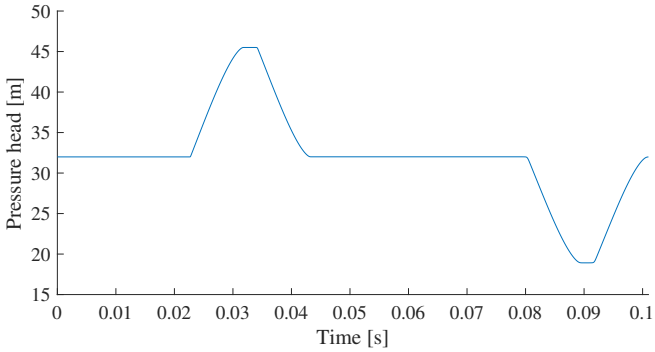

Figure 7.8: Transient pressure of the same node as the velocity profile in Figure 7.6 and Figure 7.7

Notes on the Transient Velocity Profile

When the pressure gradient used in the heat equation is replaced by the transient pressure gradient taken from the MOC simulations, a transient velocity profile is produced. As expected, the velocity profile maintains its shape while its being pushed back, and very steep velocity gradients occur near the wall. When the velocity returns to being positive, the core still holds the shape of the initial profile while a new peak occurs near the wall. The frictional forces exerted on a fluid are directly related to the velocity gradient near the wall. Although the flow rate is approximately the same as it was for the steady state case, the frictional forces will be substantially larger than in the initial case. A frictional model purely based on the bulk velocity, such as the QS model, will be unable to capture this effect. Additionally, when the bulk velocity is zero, there will still be a velocity profile, and thus a frictional loss related. From the velocity profile, it is apparent why a transient friction model is required for simulating this type of flow phenomenon.

7.2.3 Comparing Flow Rate to Original MOC

In order to evaluate the 2D velocity profile, its flow rate was computed and compared with the flow rate of the MOC from which the pressure gradient was taken. Velocity profiles and flow rates based on pressure gradients from the three different friction models were constructed. When compared to the flow rate of their respective MOC, all the friction models show large discrepancies.

Both plots in Figure 7.9 are related to the flow rate of the node adjacent to the outlet. In essence, the flow rate should be zero, or approximately zero because it is right next to the closed valve. Figure 7.9 **(a)** shows the flow rate of the heat equation based on data from the QS MOC simulation and the original flow rate from the QS MOC. The flow rate from the MOC goes to zero, and has minor peaks, both negative and positive, every time the pressure wave passes. Unequally, the flow rate, computed from the heat equation, does not go to zero and appears to increase throughout the simulation. At $1.5s$ the velocity is

nearly 17% of the initial velocity. This is unacceptably large. In addition, it is unphysical as no water can actually flow through the closed valve.

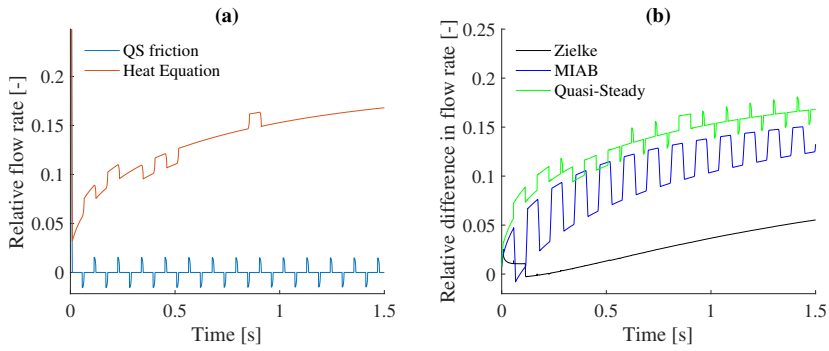

Figure 7.9:
(a) shows flow rates for MOC (QS) and the respective heat equation. The flow rates are normalized by the initial, steady state flow rate Q_0
(b) shows the difference in flow rates between MOC and the heat equation for various friction models. The flow differences are normalized by the same initial, steady state flow rate Q_0
Both figures are related to a node located $0.074m$ from the outlet

Figure 7.9 **(b)** shows the difference between the flow rate computed from the heat equation and the flow rate of the MOC for the three different friction models. To clarify, the plot shown for Zielke is $(Q_{heatEQ,Zielke} - Q_{MOC,Zielke})/Q_0$, and similar for the other two friction models. Flow rates of all the various friction models show relatively large discrepancies. Zielke's friction model show a closer match to its origin, however the difference is still substantial, being 5% and increasing still at the end of the simulation.

An important note from Figure 7.9, is that none of the heat equation models drops all the way to zero during the initial valve closure. This is most visible in Figure 7.9, and is common for all the models.

Investigating a Smaller Time Step

The error, between the flow rate of the velocity profile from the heat equation and the MOC, could be related to the size of the time step used in the simulation. Hence, simulations were carried out for various time steps. In MOC the time step, dt, is directly computed from the spatial step. To how a variation in dt would affect the heat equation, three new MOC simulations with a QS friction model were conducted.

The pipe of the experiment was divided into $N = 1501, 501$ and 101 reaches, which in turn would be compared to the initial simulation of 1001 reaches. The smallest dt would be related to $N = 1501$ and the largest to $N = 101$.

Figure 7.10 shows that the variation in dt has little effect on the flow rate. A result which is quite surprising, as the expected outcome was that a finer time step would also mean a smaller difference between the flow rates. Interestingly, the difference in flow rate appear to increase slightly with a finer time step. Note that the difference between the

three is still fairly small.

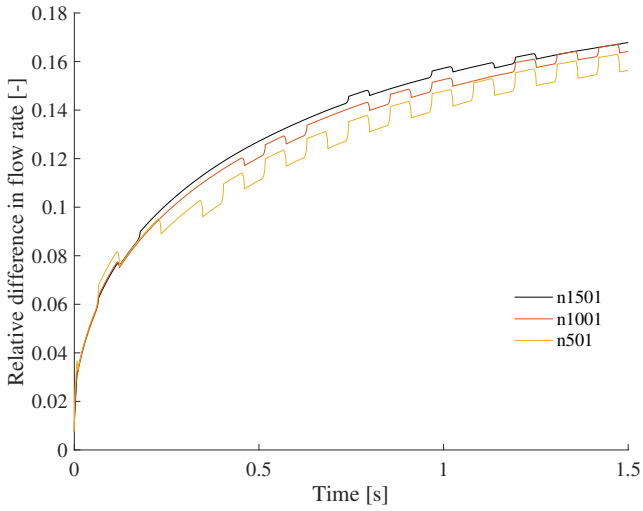

Figure 7.10: Difference in flow rate between the heat equation and the MOC (QS) divided by the initial flow rate, for a variation in time step

Further Flow Rate Investigation

Since refining the time step appeared to have little effect on the flow rate, the flow rate of node number 200, located approximately $7m$ from the inlet, was investigated. From Figure 7.11, the match is close to the initial MOC, but the error is present, and increasing throughout the simulation.

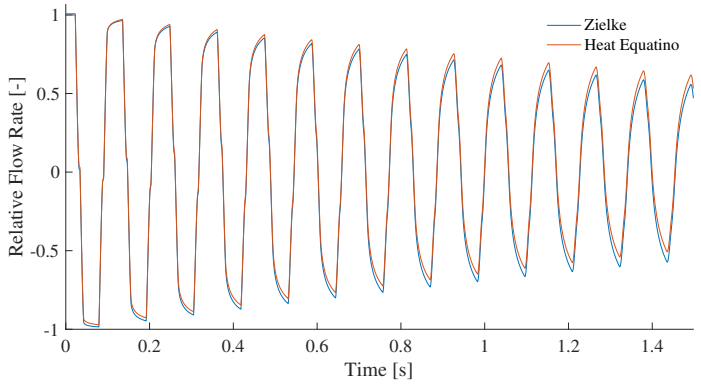

Figure 7.11: Relative flow rate of the flow obtained using the heat equation and the MOC with Zielke's friction model

Zooming in on the first few amplitudes of the flow plot of Figure 7.11, a small offset in the initial flow becomes visible, displayed in Figure 7.12 .

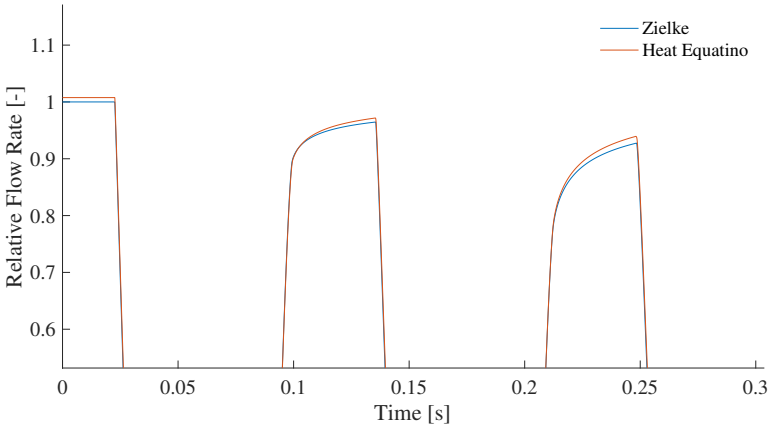

Figure 7.12: Relative flow rate of the flow obtained using the heat equation and the MOC with Zielke's friction model, zoomed in

The initial offset, visible in Figure 7.12, could be the reason none of the flow rates go to zero during the initial velocity stop. Whether it has a large effect on the error that increases throughout the simulation should be investigated. Unfortunately, due to time limitations, it will not be investigated in this thesis.

Additionally, refinement of the radial mesh was investigated, and shown to have little effect on the flow rate error that increases throughout the simulation. Leading the author to believe that the error is either related to the viscosity, or that the method is unfit for simulation of water hammer events.

Discussion; Velocity Profile

Although the velocity profile was able to take on the characteristics that were expected, it was unable to correctly model the flow rate. For all three friction models, the error related to the flow rate was unacceptably large. None of the velocity profiles flow rates go down to zero during the initial valve closure. Adjacent to a closed valve the flow rate should be zero, or at least approximately zero. Then, the error was increasing throughout the simulation for all the models. It appears to be converging towards an unknown value. However, longer simulations would be needed to determine whether there is such convergence, and the simulation length was predetermined by the experiment by Bergant et al. [2].

The cause of this error is supposedly related to the large and sudden changes of the pressure. If one studies the transient pressure plots in Figure 7.1 to Figure 7.3, Zielke's model is more rounded whereas the two other models have squared peaks. Since the error in Zielke's model is much smaller than that of the others, it seems that the numerical scheme more easily follows the softer pressure changes related to Zielke's model.

Considering the error seems to be related to the abrupt pressure changes related to a water hammer, it is likely that the heat equation would perform much better when applied to less severe transient events. Current results considered, applying this technique for a water hammer simulation is not promising. However, the cause of the error should be investigated further.

Another possible source of the error in the flow rate, could be related to the steady state velocity profile, which is largely influenced by the viscosity. The viscosity was computed from the Reynold's number given by Bergant et al. [2], and it is possible that choosing a better viscosity could impact both the steady state velocity profile, and the error that is increasing throughout the simulation.

7.3 Turbulent Velocity Profile

If the heat equation is to be applicable as a translator between 1D and 3D simulations of hydro power stations, it needs to be valid for turbulent flow. This poses an immediate challenge as the 2D profile is generated based on laminar flow assumptions.

The following results are based on the reduced version of NS momentum equation in section 5.3, and values presented in subsection 6.3.1. Again, the values are chosen at will, and so this simulation does not have experimental data for comparison. A velocity profile was made by the power-law, presented in section 2.6. This was used as a reference to see whether a time-averaged turbulent velocity profile could be made by numerically solving the reduced NS momentum equation.

Modified Viscosity

The viscosity was modified empirically, and the constants of Equation 6.1 was altered until the velocity profile from the heat equation matched with the velocity profile from the power-law. The position dependent viscosity is graphically represented in Figure 7.13. This specific set of coefficients was seen to work well for this specific simulation.

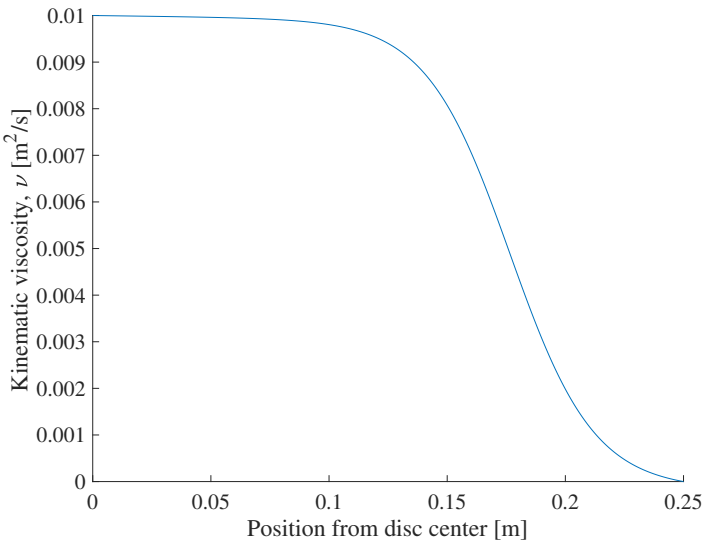

Figure 7.13: Viscosity Relative to position from center

Velocity Convergence

The simulation run until the velocities related to all points along the radius converged. Convergence is slowest in the center, and it is displayed in Figure 7.14.

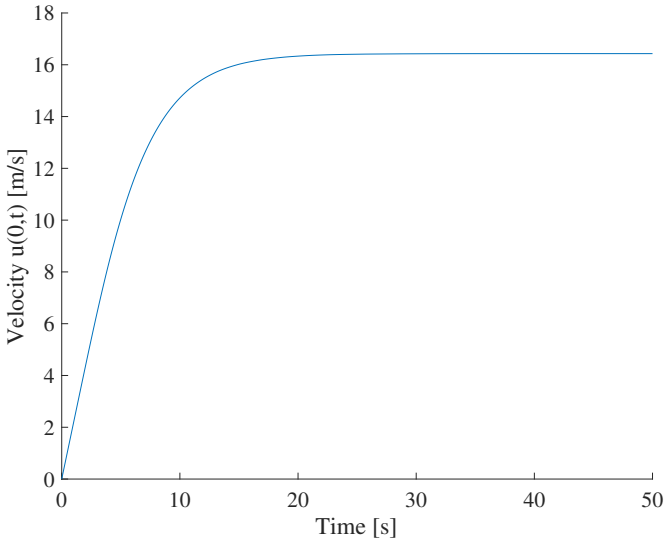

Figure 7.14: Velocity change at the center of the pipe cross-section

Velocity Profile Comparison

After testing out various values for the modified viscosity, the shape of the velocity profile seems to be a decent approximation of a time-averaged turbulent velocity profile, as can be seen in Figure 7.15. There are however some differences. First and foremost, both cases are based of a set of conditions, including the original flow rate, Q_0. The value of the original flow rate, as well as the flow rate obtained by the PDE-solver Q_{pdepe}, and the power law $Q_{powerlaw}$ is listed below.

- $Q_0 = 2.76071 m^3/s$
- $Q_{pdepe} = 2.76073 m^3/s$
- $Q_{powerlaw} = 2.75856 m^3/s$

At the pipe centerline, $x = 0$ in Figure 7.15, there is not a zero gradient for the power law, according to the literature this is one of the points where the power law fails. For the profile generated by the heat equation and the modified viscosity however, the velocity gradient on the centerline is indeed zero. The flow rate from the heat equation velocity profile is also closer to the initial flow rate than the power-law velocity profile.

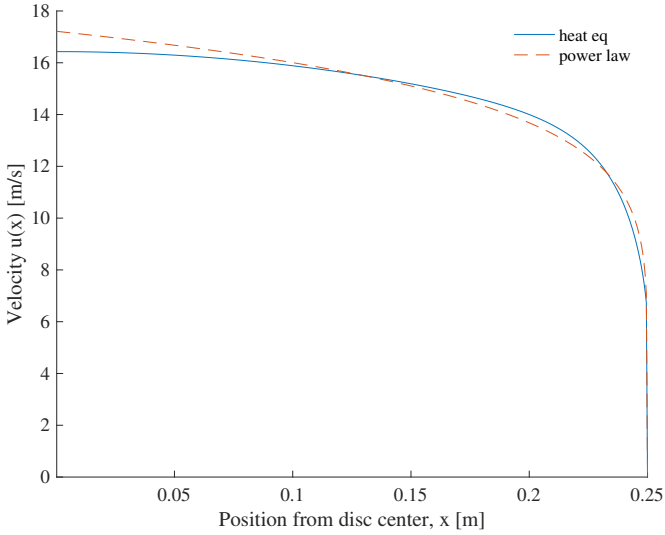

Figure 7.15: Comparing velocity profile constructed with heat equation and power law of $n = 7$

Discussion; Turbulent Profile

For this simulation, the viscosity was modified through trial and error until a velocity profile was matching the initial results. Eventually, both flow-rate, was showing a good match with the theoretical velocity profile, and the initial flow rate. However, when the radial refinement was changed, the velocity profile no longer showed a good match, and once again the viscosity required altering.

Although, the model appears to be somewhat accurate for a steady state case, it is of little interest unless it also can handle a varying pressure gradient and still produce the correct flow rate and velocity profile. The laminar simulations in this study show that for the time varying pressure gradient, there is a large error in the flow rate from the velocity profile. For a turbulent simulation, the same problem is likely to be reoccurring.

7.4 Discussion

7.4.1 Heat Equation as Translator

The reason for using this method to produce a velocity profile with data from the 1D model, is to possibly provide a method for transferring data from 1D to 3D in a coupled model. If the velocity profile from this method is going to be used as a translator at the boundaries, it is crucial that it preserves the flow properties.

From the results, this method produces a velocity profile which gives an erroneous flow rate. The cause of the error could be that the numerical method is unable to follow the large and abrupt changes related to the water hammer. It could also be related to the viscosity, computed based on the Reynold's number from [2]. The latter would have been investigated further if more time was available to the author.

Although the heat equation has a large error for the water hammer simulation, as seen in section 7.2, it should still be tested for less severe transient events. There is no documentation on how the model would fare with such conditions, and it would be interesting to study. The objective of this project is to help simulations for investigating fatigue loads on turbines. Fatigue loads can arise during a variety of flow conditions, but the loads that occur during normal operating conditions are the most interesting. Perhaps a model does not need to successfully all types of fluid events, such as a water hammer, if the purpose is to investigate normal operating conditions.

7.4.2 Relevance of unsteady friction

In the set up by Bergant et al. [2], accounting for transient friction is necessary in order to model a water hammer event correctly. Again, this is a water hammer in a thin pipe with laminar flow conditions. The literature study presented in section 3.1 refers to a study where a criterion based on the friction factor, size of the pipe and the speed of the flow is established. According to the study, if the pipe system and Reynold's number is large enough, a transient friction model will only be good for increased computational time. It may even lead to over-damping the pressure amplitudes in the case of a water hammer simulation.

The criterion formulated by Duan et al. [16] is made for water hammer simulations. During normal operating conditions, it is likely that the effects of transient friction will be less or even negligible. Relevance, and how the friction model impact transient phenomena that occur during normal operating conditions is not addressed, and would certainly be interesting to investigate. Many problems that occur for hydropower stations are related to fatigue loads inflicted during normal operation. If a simulation is designed for investigating this, a QS friction model may be the best suited model.

NTNU's hydro power laboratory has pipes of a smaller scale than a hydro power station, but a larger diameter than the on used by Bergant et al. [2]. It would be interesting to test the various 1D friction models against both water hammer, and flow with less severe pressure pulsations, to see whether a transient friction model is necessary for a system of this scale.

Initially, the transient friction models were introduced for more accurate modelling. If a certain criterion related to system size and Reynold's number is met, a transient friction

model could prove to be nothing but extra computational load. In that case, using a QS model would save computational time and possibly memory use depending on the transient friction model considered.

The overall notion is that for a large system, such as a high head Francis turbine, a QS model may be the better option. However, for intermediate scale systems, such as the hydro power laboratory at NTNU, the choice of friction model should be based of experimental results.

Validating the frictional model based on experimental results is a natural step before proceeding with a coupled simulation. A coupled model cannot be more accurate than its least accurate component, and if the friction model of the 1D model has not been tested, assessing the potential coupled model would be increasingly difficult.

7.4.3 Coupling & Notion Towards Further Work

An obvious, and critical concern for coupled models, is the coupling technique. The partly overlapped coupling (POC) used by Zhang and Cheng [39] appears to be the most viable option. It does not require interpolation, and its author already obtained promising results. The 1D and 3D model would still communicate section average variables to each other. It is for this exact purpose the heat equation could be useful. Possibly the 2D velocity profile could be used to produce a variation along a pipe-radius. Unfortunately, the results from the heat equation models in this work had a large error related, and would probably make a coupled model less accurate.

A Notion Towards Further Work

The documentation of 1D-3D coupled models is still lacking, and there are many angles that demands consideration which has not been mentioned in this work. Further work should consist of more testing as experimental comparison is dearly needed. If NTNU's hydropower laboratory is to be utilized, the testing should be divided into two main parts. Firstly, the unsteady friction model of the 1D MOC should be inspected. This can be done by testing for both a water hammer simulation, and a less severe transient event, for example by small periodic variation of the flow rate. The notion from the literature study is that accounting for transient friction becomes less relevant for larger pipe systems and higher Reynold's number, and so its relevance should be investigated.

Additionally, experiments for a waterway with a bifurcation could provide insightful information. Many hydropower stations have complicated waterways, which provides additional reflection points for pressure pulsations. A 1D model could completely cover the waterway with a simple bifurcation, and would certainly be the most efficient way to perform this type of simulation. However, this could also be used to test a 1D-3D coupled model, using 3D CFD to cover the branching point. This would, hopefully, provide useful information on the coupled models performance, and the results could be compared to both experimental data and the pure 1D model. It would be interesting to see whether the model would be able to conserve the frequencies and amplitudes of the pressure pulsations, or if some information would get lost in translation.

Chapter 8

Conclusion and Further Work

Simulations using the 1D MOC were successfully carried out with three different friction models, QS, MIAB and Zielke's model. The results were validated against a publication by Bergant et al. [2]. The results showed that transient friction must be accounted for, when conducting water hammer simulations for laminar flow in a thin pipe. However, a study by Duan et al. from 2012 states that transient friction looses its relevance as the scale of the system and Reynold's number increases. In addition, severe transient events, such as a water hammer, may exaggerate the need of a transient friction model. In conclusion, the choice of friction model should be based on the criterion by Duan et al. [16], or ideally based on experimental data.

A reduced form the NS momentum equation was applied to produce a 2D velocity profile with data from the 1D MOC. The possibilities of using this method as a 1D-3D translator was investigated. The transient pressure gradient was retrieved from the MOC, and a time-varying velocity profile was generated. From the profile, the steep gradients and back flow, that occur during a water hammer, were clearly visible. The flow rate was not conserved in the new velocity profile in a satisfactory manner. Seemingly, the error is related to the viscosity or the steep and abrupt changes of the pressure, and should be investigated further. By the current results, the error related to the method is not tolerable.

The method described in the previous paragraph was also applied to produce a turbulent velocity profile. In order to realize the turbulent profile, the viscosity was modified by trial and error. The velocity profile was generated for steady state, fully developed pipe flow. Arriving at the correct viscosity was a tedious process. Eventually, a steady state velocity profile was produced, and it showed good match with the analytical profile, and the initial flow rate. The modified viscosity appeared to only hold for the mesh size it was produced for. Changing the radial refinement gave large variations in the results, for the same viscosity function. In summary, the method does not appear promising for turbulent flow, although it should be tested against transient conditions before being completely disregarded.

8.1 Further Work

One of the main limitations when setting up the simulations, was the lack of experimental results for comparison. As such, the further work suggests a simple experiment which could provide insightful information in terms of a 1D-3D couple simulation.

A system consisting of one inlet, one outlet and a blind tunnel could be considered. Experiments should be performed for both a water hammer, and a periodic flow variation. This would provide two types of transient events, which can be useful when evaluating the simulation models. The blind tunnel provides an additional reflection point for the pressure waves, which makes it more challenging for the simulation models. Firstly, the experiment should provide information on the friction model of the 1D MOC. Thus, the one should start by doing a full 1D simulation of the experimental rig. A precise friction model is crucial if the 1D model is to be viable for a coupled simulation.

If the 1D model is able to successfully model the transient events, the bifurcation could be replaced by a 3D CFD model, attempting a coupled simulation of the experimental rig. Relevant results from the 1D simulation, in addition to the experiment would then be available, and the coupled 1D-3D model could be thoroughly investigated. For the set up of the 1D-3D coupled model, the POC method by Zhang and Cheng [39] would be recommended. In terms of software, it can be implemented in ANSYS CFX and FLUENT using the CEL programming language. This is a very specific case, and there are certainly different approaches that could further the studies on 1D-3D coupled simulations. However, the overall notion is that the field is in need of experimental investigation.

Bibliography

[1] M. Farstad Perkunder, T.K. Nielsen, and C. Faudot. Investigation of fluid transients in a penstock attached to a francis turbine rig using seismic interferometry. Institute of Physics Publishing, 2019.

[2] Anton Bergant, Angus Ross Simpson, and John Vìtkovsk. Developments in unsteady pipe flow friction modelling. *Journal of Hydraulic Research*, 39(3):249–257, 2001.

[3] Pål-Tore Storli and Torbjørn K Nielsen. Transient friction in pressurized pipes. i: Investigation of zielke's model. *Journal of Hydraulic Engineering*, 137(5):577–584, 2011.

[4] Peter Dörfler, Mirjam Sick, and André Coutu. *Flow-induced pulsation and vibration in hydroelectric machinery: engineer's guidebook for planning, design and troubleshooting*. Springer Science & Business Media, 2012.

[5] EB Wylie and VL Streeter. Fluid transients corrected edition ed. *Thomson-Shore, Dexter, MI, United States of America*, 1983.

[6] Magnus Farstad Perkunder, Torbjørn K Nielsen, and Celine Faudot. Investigation of fluid transients in a penstock attached to a francis turbine rig using seismic interferometry. In *Journal of Physics: Conference Series*, volume 1266, page 012010. IOP Publishing, 2019.

[7] NMC Martins, B Brunone, S Meniconi, HM Ramos, and DIC Covas. Cfd and 1d approaches for the unsteady friction analysis of low reynolds number turbulent flows. *Journal of Hydraulic Engineering*, 143(12):04017050, 2017.

[8] Y Cengel and J Cimbala. Fluid mechanics whith studenr resources, 2009.

[9] Pål-Tore Storli. Transient friction in pressurized pipes; the water hammer phenomenon. 2010.

[10] John P Vítkovskỳ, Anton Bergant, Angus R Simpson, and Martin F Lambert. Systematic evaluation of one-dimensional unsteady friction models in simple pipelines. *Journal of Hydraulic Engineering*, 132(7):696–708, 2006.

[11] B Brunone, M Cacciamani, F Calabresi, and M Ferrante. An investigation on unsteady-state friction in laminar flow. *Pumps, electromechanical devices and systems applied to urban water management*, 2003.

[12] Alan E Vardy and Jim MB Brown. Transient, turbulent, smooth pipe friction. *Journal of Hydraulic Research*, 33(4):435–456, 1995.

[13] Mohamed S Ghidaoui, Ming Zhao, Duncan A McInnis, and David H Axworthy. A review of water hammer theory and practice. *Applied Mechanics Reviews*, 58(1): 49–76, 2005.

[14] Werner Zielke. Frequency-dependent friction in transient pipe flow. 1968.

[15] Sharon Mandair, Bryan Karney, Robert Magnan, et al. Comparing pure cfd and 1-d solvers for the classic water hammer models of a pipe-reservoir system. In *WDSA/CCWI Joint Conference Proceedings*, volume 1, 2018.

[16] H-F Duan, MS Ghidaoui, PJ Lee, and YK Tung. Relevance of unsteady friction to pipe size and length in pipe fluid transients. *Journal of hydraulic engineering*, 138 (2):154–166, 2012.

[17] Mark Stephens, Angus R Simpson, Martin F Lambert, and John P Vítkovskỳ. Field measurements of unsteady friction effects in a trunk transmission pipeline. In *Impacts of Global Climate Change*, pages 1–12. 2005.

[18] Nuno MC Martins, Alexandre K Soares, Helena M Ramos, and Dídia IC Covas. Cfd modeling of transient flow in pressurized pipes. *Computers & Fluids*, 126:129–140, 2016.

[19] Arun K Trikha. An efficient method for simulating frequency-dependent friction in transient liquid flow. *Journal of Fluids Engineering*, 97(1):97–105, 1975.

[20] Toshiharu Kagawa. High speed and accurate computing method of frequency-dependent friction in laminar pipe flow for characteristics method. *JSME Int. J., Ser. B*, 49(447):2638–2644, 1983.

[21] Katsumasa Suzuki, Takayuki Taketomi, and Sanroku Sato. Improving zielke's method of simulating frequency-dependent friction in laminar liquid pipe flow. 1991.

[22] Mohamed S Ghidaoui and Sameh Mansour. Efficient treatment of the vardy–brown unsteady shear in pipe transients. *Journal of Hydraulic Engineering*, 128(1):102–112, 2002.

[23] JP Vítkovskỳ, M Stephens, A Bergant, M Lambert, and AR Simpson. Efficient and accurate calculation of zielke and vardy-brown unsteady friction in pipe transients. In *Proceedings of the 9th international conference on pressure surges*, volume 2, pages 405–419, 2004.

[24] JW Daily, WL Hankey Jr, RW Olive, and JM Jordaan Jr. Resistance coefficients for accelerated and decelerated flows through smooth tubes and orifices. Technical report, MASSACHUSETTS INST OF TECH CAMBRIDGE, 1955.

[25] UM Golia. Sulla valutazione delle forze resistenti nel colpo d'ariete. *Report n*, 639, 1990.

[26] B Brunone, UM Golia, and M Greco. Some remarks on the momentum equation for fast transients. In *Proc. Int. Conf. on Hydr. Transients With Water Column Separation*, pages 201–209, 1991.

[27] AE Vardy and JMB Brown. Transient turbulent friction in smooth pipe flows. *Journal of Sound and Vibration*, 259(5):1011–1036, 2003.

[28] B Brunone, UM Golia, and M1 Greco. Effects of two-dimensionality on pipe transients modeling. *Journal of Hydraulic Engineering*, 121(12):906–912, 1995.

[29] D Loureiro and H Ramos. A modified formulation for estimating the dissipative effect of 1d transient pipe flow. *Pumps, electromechanical devices and systems applied to urban water management*, 2003.

[30] Pål-Tore Storli and Torbjørn K Nielsen. Transient friction in pressurized pipes. ii: two-coefficient instantaneous acceleration–based model. *Journal of Hydraulic Engineering*, 137(6):679–695, 2011.

[31] HF Duan, S Meniconi, PJ Lee, B Brunone, and MS Ghidaoui. Local and integral energy-based evaluation for the unsteady friction relevance in transient pipe flows. *Journal of Hydraulic Engineering*, 143(7):04017015, 2017.

[32] H Lewy, K Friedrichs, and R Courant. Über die partiellen differenzengleichungen der mathematischen physik. *Mathematische Annalen*, 100:32–74, 1928.

[33] Richard Courant, Kurt Friedrichs, and Hans Lewy. On the partial difference equations of mathematical physics. *IBM journal of Research and Development*, 11(2): 215–234, 1967.

[34] Ching-Long Lin, MH Tawhai, G McLennan, and EA Hoffman. Multiscale simulation of gas flow in subject-specific models of the human lung. *IEEE Eng. Med. Biol. Mag*, 28(3):25–33, 2009.

[35] HAN Dong, Hong-wei Fang, BAI Jing, and Guo-jian He. A coupled 1-d and 2-d channel network mathematical model used for flow calculations in the middle reaches of the yangtze river. *Journal of Hydrodynamics, Ser. B*, 23(4):521–526, 2011.

[36] Albert Ruprecht, Thomas Helmrich, Thomas Aschenbrenner, and Thomas Scherer. Simulation of vortex rope in a turbine draft tube. In *Proceedings of 22nd IAHR Symposium on Hydraulic Machinery and Systems*, pages 9–12, 2002.

[37] A RUPRECHT and T HELMRICH. Simulation of the water hammer in a hydro power plant caused by draft tube surge [c]. 4th asme/jsme joint fluids engineering conference. *Honolulu, Hawaii, USA*, 2003.

[38] Sergey Cherny, Denis Chirkov, Denis Bannikov, Vasily Lapin, Vladimir Skorospelov, Irina Eshkunova, and Alexander Avdushenko. 3d numerical simulation of transient processes in hydraulic turbines. In *IOP Conference Series: Earth and Environmental Science*, volume 12, page 012071. IOP Publishing, 2010.

[39] Xiao-xi Zhang and Yong-guang Cheng. Simulation of hydraulic transients in hydropower systems using the 1-d-3-d coupling approach. *Journal of Hydrodynamics, Ser. B*, 24(4):595–604, 2012.

[40] Chao Wang, Håkan Nilsson, Jiandong Yang, and Olivier Petit. 1d–3d coupling for hydraulic system transient simulations. *Computer Physics Communications*, 210: 1–9, 2017.

[41] Dazhuan Wu, Shuai Yang, Peng Wu, and Leqin Wang. Moc-cfd coupled approach for the analysis of the fluid dynamic interaction between water hammer and pump. *Journal of Hydraulic Engineering*, 141(6):06015003, 2015.

[42] Xiao-xi Zhang, Yong-guang Cheng, Jian-dong Yang, Lin-sheng Xia, and Xu Lai. Simulation of the load rejection transient process of a francis turbine by using a 1-d-3-d coupling approach. *Journal of Hydrodynamics*, 26(5):715–724, 2014.

[43] Deyou Li, Xiaolong Fu, Zhigang Zuo, Hongjie Wang, Zhenggui Li, Shuhong Liu, and Xianzhu Wei. Investigation methods for analysis of transient phenomena concerning design and operation of hydraulic-machine systems—a review. *Renewable and Sustainable Energy Reviews*, 101:26–46, 2019.

[44] JL Yin, DZ Wang, LQ Wang, YL Wu, and XZ Wei. Effects of water compressibility on the pressure fluctuation prediction in pump turbine. In *IOP Conference Series: Earth and Environmental Science*, page 062030. IOP Publishing, 2012.

[45] Erik Os Tengs. Numerical simulation of fluid-structure interaction in high head francis turbines. 2019.

[46] Kenneth C Hall, Jeffrey P Thomas, and William S Clark. Computation of unsteady nonlinear flows in cascades using a harmonic balance technique. *AIAA journal*, 40 (5):879–886, 2002.

Appendix A

MOC with MIAB Friction Model

The governening equations, already presented in chapter 3, are repeated here [5, 9].

$$H_x + \frac{1}{g}V_t + h_f = 0 \tag{A1}$$

$$H_t + \frac{a^2}{g}V_x = 0 \tag{A2}$$

The subscripts x and t denotes the partial derivatives with respect to space and time. H is the piezometric head, x and t are the space and time variables, respectively, V is the bulk flow velocity, a is the wave propagation speed, g is the gravitational constant and h_f is the head loss per unit length.

The head loss, h_f will be divided into a quasi steady, and an unsteady term, $h_{f,q}$ and $h_{f,u}$. Presented in section 3.4 and repeated here.

$$h_f = h_{f,q} + h_f, u = f\frac{V|V|}{2gD} + \left(\frac{k_t}{g}V_t + \frac{k_x a\phi}{g}V_x\right) \tag{A3}$$

Characteristics Equations

The continuity and momentum equations (A2) and (A1) form a pair of quasi-linear hyperbolic partial differential equations in terms of two dependent variables, velocity and hydraulic-grade-line elevation, and two independent variables, distance along the pipe and time. Skipping a few steps, the equations are formed into four ordinary differential equations by the characteristics method.

$$\left.\begin{array}{l} \lambda\frac{dH}{dt} + (1+k_t)\frac{dV}{dt} + \frac{fV|V|}{2D} = 0 \\ \frac{dx}{dt} = \frac{2a}{-\phi k_x + \sqrt{k_x^2 + 4(1+k_t)}} \end{array}\right\} C^+$$
$$\left.\begin{array}{l} \lambda\frac{dH}{dt} + (1+k_t)\frac{dV}{dt} + \frac{fV|V|}{2D} = 0 \\ \frac{dx}{dt} = \frac{-2a}{\phi k_x + \sqrt{k_x^2 + 4(1+k_t)}} \end{array}\right\} C^- \tag{A4}$$

$$C^+ \qquad \Rightarrow \qquad \lambda = \frac{-\phi k_x + \sqrt{k_x^2 + 4(1+k_t)}}{2a/g}$$

$$C^- \qquad \Rightarrow \qquad \lambda = \frac{-\phi k_x - \sqrt{k_x^2 + 4(1+k_t)}}{2a/g}$$

Not accounting for transient friction, the characteristic lines would be given solemnly by the wave speed, $dx/dt = \pm a$. However the transient friction provides the slightly more complicated characteristic lines seen in Equation A4.

The ordinary differential equations (A4) are valid along the characteristic lines C^+ and C^-. This impose the need of initial values as $x = ct - x_0$, for getting a solution for the domain. A solution can be found using the finite-differences equations.

Modifying Equation A4 the following relation is obtained.

$$C^+ \qquad \Rightarrow \qquad \frac{dx}{g} = \frac{2a/g}{-\phi k_x + \sqrt{k_x^2 + 4(1+k_t)}} dt$$

$$C^- \qquad \Rightarrow \qquad \frac{dx}{g} = \frac{-2a/g}{\phi k_x + \sqrt{k_x^2 + 4(1+k_t)}} dt$$

The above relation combined with Equation A4 produces the following relation for C^+ and C^- respectively.

$$dH + \frac{(1+k_t)2a/g}{-\phi k_x + \sqrt{k_x^2 + 4(1+k_t)}} dV + f\frac{V|V|}{2gD} dx = 0 \tag{A5}$$

$$dH - \frac{(1+k_t)2a/g}{\phi k_x + \sqrt{k_x^2 + 4(1+k_t)}} dV + f\frac{V|V|}{2gD} dx = 0 \tag{A6}$$

Introducing the cross-sectional pipeline area A and the average discharge $Q = V * A$ Integrating the equations along the characteristic lines, from A to P for C^+ and from B to P for C^-.

$$C^+ : H_P = H_A - B^+(Q_P - Q_A) - RQ_A|Q_A| \tag{A7}$$

$$C^- : H_P = H_B + B^-(Q_P - Q_B) + RQ_B|Q_B| \tag{A8}$$

These two compatibility equations are basic algebraic relations that describe the transient propagation of pressure head and flow in a pipeline. The notation of B^+, B^- and R has been introduced to make the equations simpler.

$$B^+ = 2\frac{a}{gA}\frac{(1+k_t)}{(-\phi k_x + \sqrt{k_x^2 + 4(1+k_t)})}$$

$$B^- = 2\frac{a}{gA}\frac{(1+k_t)}{(\phi k_x + \sqrt{k_x^2 + 4(1+k_t)})}$$

$$R = f\frac{\Delta x}{2gDA^2}$$

These equations must hold for steady flow where $Q_A = Q_P = Q_B$ and $RQ_A|Q_A|$ is the steady-state friction term.

The solution to a transient problem usually begins with steady-state conditions at time zero, so that H and Q are known initial values. Then H and Q are found for each grid point where $t = \Delta t$, then $t = 2\Delta t$ and so on. At any interior grid intersection point, section *i*, the two compatibility equations are solved simultaneously for Q_{P_i} and H_{P_i}. Equations (A7) and (A8) may be written in a simple form,

$$C^+ : H_{P_i} = C_P - B^+ Q_{P_i} \tag{A9}$$

$$C^- : H_{P_i} = C_M + B^- Q_{P_i} \tag{A10}$$

in which C_P and C_M are always known from the variables of the previous time step.

$$C_P = H_{i-1} + B^+_{i-1} Q_{i-1} - RQ_{i-1}|Q_{i-1}| \tag{A11}$$

$$C_M = H_{i+1} - B^-_{i+1} Q_{i+1} + RQ_{i+1}|Q_{i+1}| \tag{A12}$$

H_{P_i} can be eliminated from (A9) and (A10) which leads to the following:

$$Q_{P_i} = \frac{C_P - C_M}{B^- + B^+} \tag{A13}$$

When Q_{P_i} have been determined, then H_{P_i} can be determined from either (A9) or (A10).

The end points of the system begin influencing the interior points after the first time step. As previously mentioned, this method is dependent on knowing all values at a present time step before it can compute the next. Thus, it is necessary to introduce appropriate boundary and initial conditions.

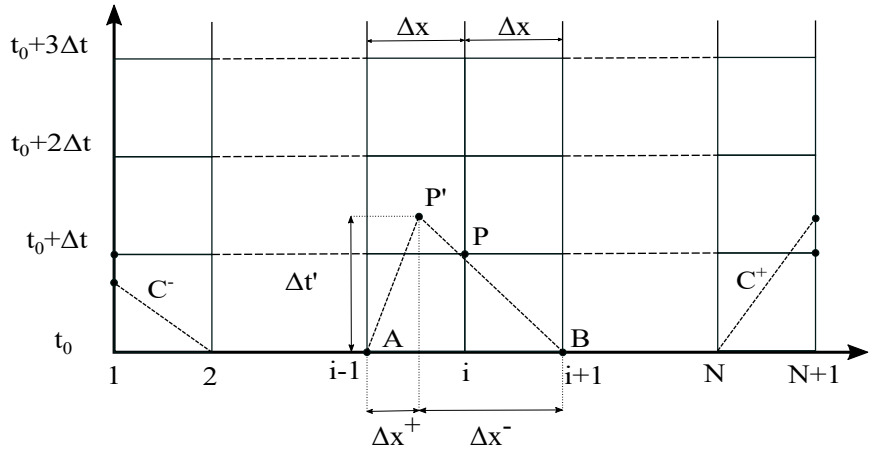

Figure A1: The grid used with MOC and MIAB friction model

Figure A1 shows how the characteristic lines deviate when transient friction is accounted for. In a MOC model with a steady state friction model, all the characteristic

lines have the same inclination. The grid is then modified so that the lines hit the same point P for the same Δt. In the MIAB model however, this is not the case, and Δt will vary and the Q_{P_i} and H_{P_i} computed from the characteristic lines does not align perfectly with the grid. A solution to this problem is interpolation, however, this may impose some numerical error on the model.

For the interpolation, the following variables needs to be determined. $\Delta t'$, Δx^+ and Δx^-. The first equation is obtained through geometric relations in Figure A1.

$$\Delta x^+ + \Delta x^- = 2\Delta x \tag{A14}$$

The second relation comes from Equation A4.

$$\frac{\Delta x^+}{\Delta t'} = \frac{2a}{-\phi k_x + \sqrt{k_x^2 + 4(1+k_t)}} \tag{A15}$$

$$\frac{\Delta x^-}{\Delta t'} = \frac{-2a}{\phi k_x + \sqrt{k_x^2 + 4(1+k_t)}} \tag{A16}$$

The subsequent equation is then found, eliminating $\Delta t'$ from Equation A15 and Equation A16.

$$\Delta x^+ \left(-\phi k_x + \sqrt{k_x^2 + 4(1+k_t)}\right) - \Delta x^- \left(\phi k_x + \sqrt{k_x^2 + 4(1+k_t)}\right) = 0 \tag{A17}$$

Hence Equation A14 and Equation A17 can be solved to determine Δx^+ and Δx^-. $\Delta t'$ can then be determined from Equation A15 or Equation A16.

With these values given, the values for H and Q can be found for the Δt and Δx associated to the grid.

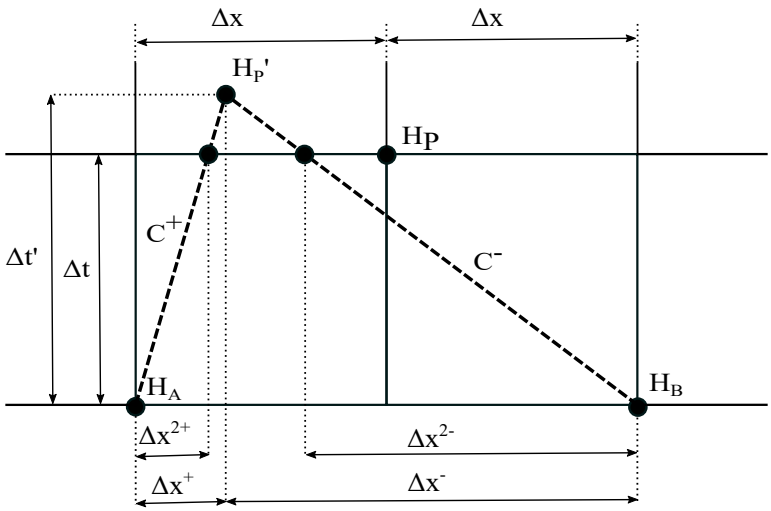

Figure A2: Illustration of the offset of H'_P compared to H_P

Figure A2 shows how the variation in the inclination of C^+ and C^- are unable to match the Δt and Δx of the set grid. Hence interpolation is utilized to determine H_P and also Q_P.

The coefficients Δx^{2+} and Δx^{2-} are found through geometry.

- $\Delta x^{2+} = \frac{\Delta t}{\Delta t'} \Delta x^+$
- $\Delta x^{2-} = \frac{\Delta t}{\Delta t'} \Delta x^-$

The characteristic lines are then displaced so the solution of the equations arrive exactly at the grid. As illustrated in Figure A3.

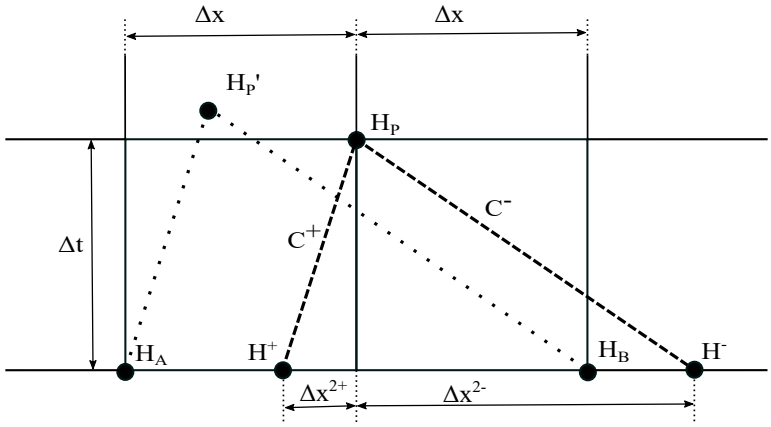

Figure A3: Illustration characteristic lines from offset H values

Figure A3 illustrates how the characteristic lines can be changed so that they provide the solution exactly at the grid of Δt and Δx. However, the values of $H^{\pm}$ and $Q^{\pm}$ of the previous time step has to be interpolated.

- If $\Delta x^{2+} > \Delta x$

$$H^{+} = H_{i-2} + \frac{2\Delta x - \Delta x^{2+}}{\Delta x}(H_{i-1} - H_{i-2}) \tag{A18}$$

$$Q^{+} = Q_{i-2} + \frac{2\Delta x - \Delta x^{2+}}{\Delta x}(Q_{i-1} - Q_{i-2}) \tag{A19}$$

- If $\Delta x^{2+} < \Delta x$

$$H^{+} = H_{i-1} + \frac{\Delta x - \Delta x^{2+}}{\Delta x}(H_{i} - H_{i-1}) \tag{A20}$$

$$Q^{+} = Q_{i-1} + \frac{\Delta x - \Delta x^{2+}}{\Delta x}(Q_{i} - Q_{i-1}) \tag{A21}$$

H^{-} and Q^{-} is determined in a similar fashion.

After all the values for $H^{\pm}$ and $Q^{\pm}$ are determined, the value of H_P can be determined from Equation A4, providing a solution of H_P exactly at the grid point. Nonetheless there will still be an error from the interpolation. The error can be made smaller by using a finer grid.

Boundary Conditions

Upstream Boundary

In the upstream reservoir there will be a constant head of H_R. This is implemented in the model by Equation A22.

$$H_{P_1} = H_R \tag{A22}$$

However, the flow rate of the system still needs to be computed. Figure A4 again shows the mismatch between the characteristic lines and the grid. At the upper boundary, only the characteristic line, C^{-} is available. The mismatch is present once again and interpolation is necessary.

From Figure A4 and C^{-} in Equation A4 the following interpolation scheme is deduced.

$$\Delta t' = \frac{\phi k_x + \sqrt{k_x^2 + 4(1 + k_t)}}{-2a}\Delta x \tag{A23}$$

Afterwards Δx^{-} is found through geometric relations seen in Figure A4. As the characteristic line may be both steeper and less steep than the inclination $\Delta t/\Delta x$, the point H^{-} may be either left or right of the point, H_2. Hence, the interpolation has to be conducted in the following manner.

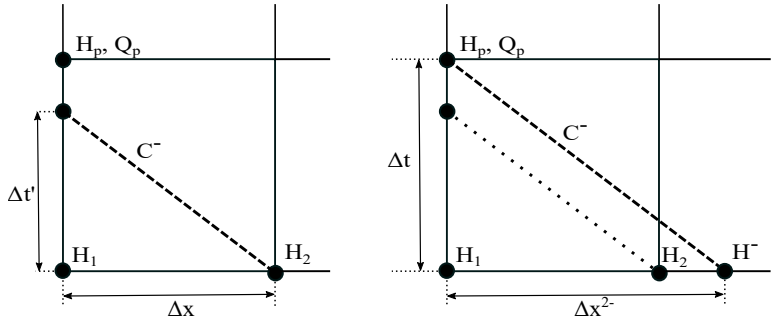

Figure A4: Illustration of upstream boundary mismatch, displacement of characteristic line C^-

- If $\Delta t' < \Delta t$

$$H^- = H_2 + \frac{\Delta x^{2-} - \Delta x}{\Delta x}(H_3 - H_2) \tag{A24}$$

$$Q^- = Q_2 + \frac{\Delta x^{2-} - \Delta x}{\Delta x}(Q_3 - Q_2) \tag{A25}$$

- If $\Delta t' > \Delta t$

$$H^- = H_1 + \frac{\Delta x^-}{\Delta x}(H_2 - H_1) \tag{A26}$$

$$Q^- = Q_1 + \frac{\Delta x^-}{\Delta x}(Q_2 - Q_1) \tag{A27}$$

After the interpolation scheme is used to determine the values for H^- and Q^-, Q_P is found using Equation A4.

Downstream Boundary

There exist several equations for describing the flow through a valve. The one used in this model is deduced by Wylie and Streeter (1983). The outflow equations is presented below.

$$Q' = -B^+ Cv + \sqrt{(B^+ Cv)^2 + 2CvC_P} \tag{A28}$$

Cv is defined so that $C_v = (Q_0\tau)^2/(2H_0)$. The dimensionless valve opening, τ is defined so that $\tau = 1$ for open valve steady flow and $\tau = 0$ for a closed valve. How τ approaches 0 can be simulated with many different equations. For this model it goes from 1 to 0 linearly with the equation $\tau = 1 - \frac{t}{t_c}$, in which t_c is the closing time.

Similarly to the upstream boundary, the characteristic line used for may not match the static grid, illustrated in Figure A5.

The mismatching characteristic line is once again modified, so it starts from a point in the lengthwise direction, so it can be solved exactly at the point H_P. Interpolation is used to determine the value of H^+. The interpolation scheme is mathematically presented subsequently.

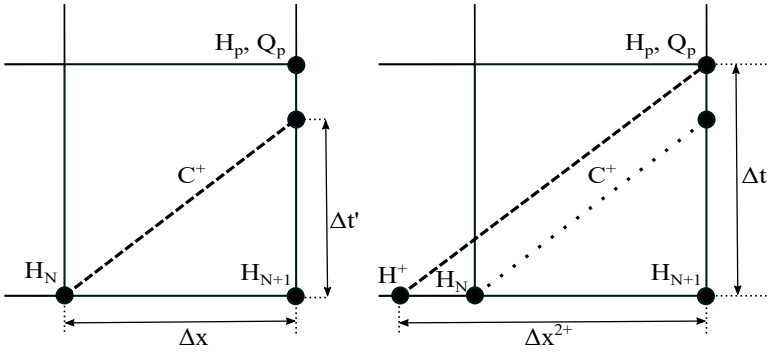

Figure A5: Illustration of downstream boundary mismatch, and quantities for interpolation

The time step $\Delta t'$ is determined from Equation A4, so that

$$\Delta t' = \frac{-\phi k_x + \sqrt{k_x^2 + 4(1+k_t)}}{2a}\Delta x \tag{A29}$$

Obtaining Δx is then done through geometric considerations, $\Delta x^+ = (\Delta t/\Delta t')\Delta x$

Once again, H^+ may be either left or right of H_N depending on the inclination of the characteristic line. This is accounted for by the following equations.

- If $\Delta t' < \Delta t$

$$H^+ = H_{N-1} + \frac{2\Delta x - \Delta x^+}{\Delta x}(H_N - H_{N-1}) \tag{A30}$$

$$Q^+ = Q_{N-1} + \frac{2\Delta x - \Delta x^+}{\Delta x}(Q_N - Q_{N-1}) \tag{A31}$$

- If $\Delta t' > \Delta t$

$$H^+ = H_N + \frac{\Delta x - \Delta x^+}{\Delta x}(H_{N+1} - H_N) \tag{A32}$$

$$Q^+ = Q_N + \frac{\Delta x - \Delta x^+}{\Delta x}(Q_{N+1} - Q_N) \tag{A33}$$

After H^+ and Q^+ has been correctly interpolated, the new Value for H_P is computed using Equation A4.

Appendix B

Detailed explanation on how to treat pipe variations, bifurcations and change in diameter, in the method of characteristics.

Complex Systems

For systems containing more than one pipeline, the interior section of each pipeline is treated independently of other parts of the system at each instant of time. Each boundary condition is treat independently of other parts of the system at each instant of time. The end conditions of each pipeline must interface with adjoining pipelines or with other boundary elements. This section covers multi-pipe systems and additional boundary conditions.

Series Connection

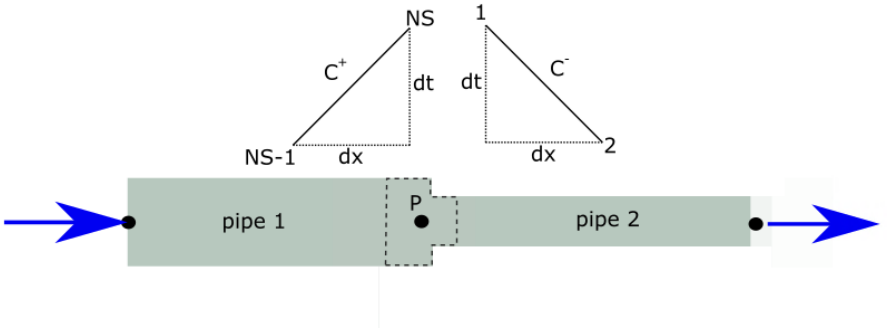

Figure B1: Series Connection redrawn from [5]

Figure B1 shows a pipeline with a change in diameter, however the method applies equally well to a change in roughness, thickness or constraint condition. At the intersection, equation (4.9) is available for pipe 1 and equation (4.10) is available for pipe 2. Continuity and the condition for a common hydraulic grade-line provide the following two equations.

$$Q_{1,NS} = Q_{2,1}, \quad H_{1,NS} = H_{2,1} \tag{B1}$$

Solving these together with equations (4.9) and (4.10) gives.

$$Q_{2,1} = \frac{C_{P_{1,NS-1}} - C_{M_{2,1}}}{B_1 + B_2} \tag{B2}$$

Branch Connection

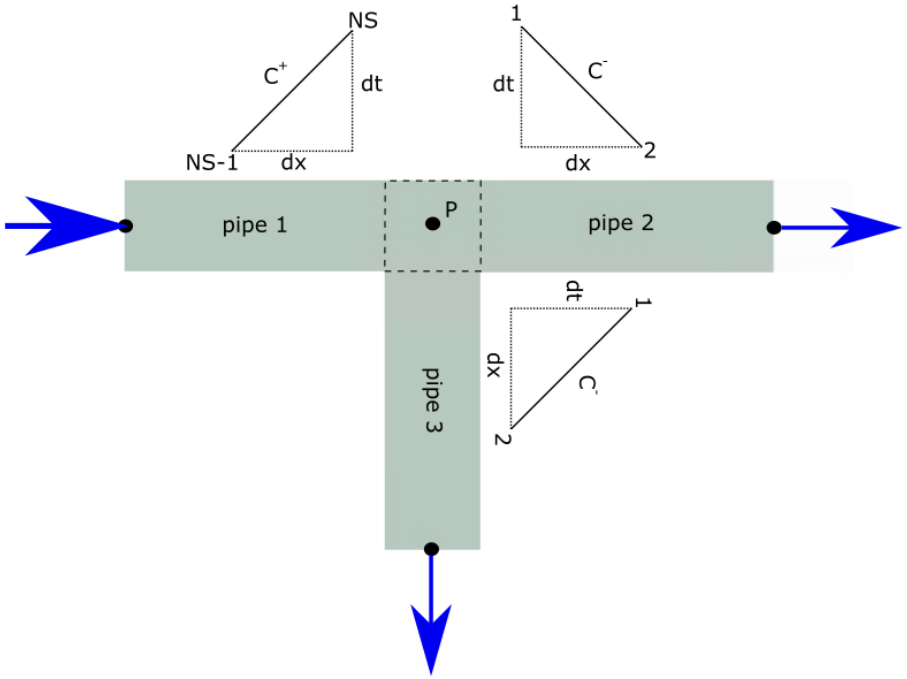

Figure B2: Branched junction redrawn from [5]

Figure B2 depicts a simple branched connection. To solve this system, the continuity equation is used, a common head is assumed when minor effects area neglected, and the compatibility equations, (4.9) and (4.10), are needed in each pipe. This gives the following equations:

$$
\begin{aligned}
H_P = H_{1,NS} = H_{2,1} = H_{3,1} \\
Q_{P_{1,NS}} = -\frac{H_P}{B_1} + \frac{C_{P_{1,NS-1}}}{B_1} \\
Q_{P_{2,1}} = +\frac{H_P}{B_2} - \frac{C_{M_{2,1}}}{B_2} \\
Q_{P_{3,1}} = +\frac{H_P}{B_3} - \frac{C_{M_{3,1}}}{B_3}
\end{aligned}
$$

A summation where the mass flow rates cancel out provides a simple solution for the common head H_P.

$$H_P = \frac{C_{P_1}/B_1 + C_{M_2}/B_2 + C_{M_3}/B_3}{1/B_1 + 1/B_2 + 1/B_3} \tag{B3}$$

Appendix C

3D Simulation

In certain sections of a hydro power station, there will be sections where the efficient 1D model falls short. Areas, such as the runner and the draft tube, will have strong 3D effects. Therefore, doing a full 3D simulation on them is necessary. However, fully simulating a hydro power station in 3D is unfeasible and probably unnecessary if one can combine the 1D model of the conduits to the 3D model in the more complex sections. To reduce computational costs, some researchers have focused their interest entirely on simulating the hydraulic machine.

Start-up, shutdown and load variations are processes where transient events are present. For accurate simulation of such events in 3D CFD, four issues arise [43].

- How to model turbulent flow
- Guide vane movement
- Unsteady boundary conditions at inlet and outlet
- Compressible simulation, state equation

Serious turbulent flow within the hydraulic machinery has a strong influence on the accuracy of the transient flow simulation. According to Li et al. (2019) simpler turbulence models are not accurate enough, and Large Eddy Simulation (LES) should be used to simulate the unsteady turbulent flow.

Several methods to model guide vane movement exist, and commercially available software such as ANSYS Fluent and CFX have a set of methods already programmed.

The accuracy of the model is influenced by the inlet and outlet conditions. In some cases, experimental data is available, and the boundary conditions can be based of them. This provides relatively high accuracy, however, one cannot always rely on experimental data to be available. In the absence of experimental data, inlet and outlet the pressure is set to be unsteady. Usually, total pressures at the inlet are approximately replaced by static pressures at the inlet.

In 3D CFD, making the assumption of an incompressible fluid is often reasonable. That is not the case for certain transient events such as water hammer. Yin et al. (2012) found compressible simulations are able to capture large pressure fluctuations, and the lower frequencies in the pressure signal. In conclusion, considering water compresssibility is strongly recommended [44]. Therefore, an equation of state must be added.

Zhang and Cheng (2012) presented two methods for constructing these equations, by defining a Density Function (DDF) and by Modifying the Ideal Gas Law (MIGL). The latter method is relatively simple to implement. However, it is unreliable in terms of its

physical meaning. Furthermore, it must be solved with the energy equation, demanding more computational resources than the DDF. DDF is an explicit scheme, so it will have good accuracy with sufficiently small time step. DDF was chosen as the preferred method by the authors [39]. In DDF, the density is modelled as a function of the pressure. Neglecting the pipe elasticity and the small changes in the wave propagation speed, a, the equation of state is expressed mathematically in the following way.

$$\rho = \rho_0 e^{(p-p_0)/\rho_0 a_0^2} \tag{C1}$$

ρ is the density, p is the pressure, and the subscript 0 denotes the reference value.

Model Order Reduction

The current bottleneck of 3D CFD is the computational demand. Increasing the efficiency would provide a more practical model. Efficiency is usually gained at the cost of accuracy. However, there are methods where one can exploit certain characteristics, such as periodical effects or geometrical features, to provide a faster model without losing too much accuracy.

The technique of Model Order Reduction (MOR) essentially reduces the complexity of the simulation for the purpose of making it more efficient. MOR focuses on the input and output parameters relevant to the project, constructing a transfer function which can substitute for the actual simulation. The method requires large amounts of data. This technique is particularly well suited for structural analysis subjected to periodic effects. For a fluid-structure-interaction simulation by Tengs (2019), the results were almost identical to solving the full structure model. Although his research is promising, it is still a work in progress [45].

Reducing the model in the CFD model is also possible, but more complicated. The linear models used for structural analysis creates matrices that are easier to work with, wherein the CFD holds many nonlinearities making MOR more complicated. However, in turbomachinery, one can exploit the unsteady flow features that are periodic in time. Hall et al. (2002) used Fourier series to represent the unsteady flow conservation variables. This assumption leads to a harmonic balance form of the Euler or Navier-Stokes equations, which can be solved using CFD. In the analysis by Hall et al., the method proved to be one to two orders of magnitude faster than conventional CFD simulations. The computational results demonstrate that even strongly nonlinear flows can be modelled to engineering accuracy. In some cases, it was also found that fluid nonlinearities area found to be important for surprisingly small blade vibrations [46].

Appendix D

Matlab Script for MOC QS friction

```
close all
clear all
clc

tic
cpuT=cputime;

%---------------Defining Variables-----------------%
    %%%%Re = 1870
N = 1001;       %grid boxes
a = 1319;       %wave propagation speed
Hr = 32;      %reservoir pressure head for BC
D = .0221;       %pipe diameter
A = .25*pi*D^2;       %crossectional area
g = 9.8066502;       %gravitational const 9.8066502
L = 37.23;       %Pipelength
f = .0345;       %Darcy-Weisbach friction factor
NS = N+1;        %number of grid points
tc = 0.009;        %closing time
tend = 1.5;
rho0 = 999.057;     %water density at 15.5 Celsius
dx = L/N;
dt = dx/a; %at the Courant boundary, could be smaller
tau = 1;        %initial valve opening
t = 0;      %time in the beginning
Em = 1.5;       %taken from example in Streeter
R = f*dx/(2*g*D*A^2);
B = a/(g*A);

Nvector = 1:NS;
x = 0:dx:L;

%---------------Initial values-----------------%
V0 = .1;
```

```
Q0(1:NS) = A*V0;
H0(1:NS) = Hr - f*dx*(Nvector-1).*Q0.*abs(Q0)/(2*g*A^2*D);

figure(1)
subplot(2,1,1)
plot(x,H0);
title('initial pressure through pipe')
axis([0 L Hr*.999 Hr]);
subplot(2,1,2)
plot(x,Q0);
axis([0 L 0 Q0(1)*1.1]);
title('initial volume flow through pipe')

Q=Q0;
H=H0;

Qnew=zeros(1,NS);
Hnew=zeros(1,NS);


P=1;

timestep=1+floor((tend/dt));
time=linspace(0,tend,timestep);


for i = 0:dt:tend
    %---------------Interior points------------------%
    Cp = H(1:NS-1) + B*Q(1:NS-1) - R*Q(1:NS-1).*abs(Q(1:NS-1));
    Cm = H(2:NS) - B*Q(2:NS) + R*Q(2:NS).*abs(Q(2:NS));
    Hnew(2:NS-1) = .5*(Cp(1:NS-2)+Cm(2:NS-1));
    Qnew(2:NS-1) = (Hnew(2:NS-1)-Cm(2:NS-1))/B;

    %---------------Upper boundary------------------%
    Hnew(1) = Hr;
    Qnew(1) = (Hnew(1)-Cm(1))/B;
    if t <= tc
        tau=(1-(1/tc)*t)^Em;
    else
        tau=0;
    end

    %---------------Lower boundary------------------%
    Cv = (Q0(1)*tau)^2/(2*H0(NS));
    if B*Cv+2*Cp(NS-1) < 0
```

```
        Qnew(NS) = -B*Cv - sqrt(abs((B*Cv)^2+2*Cv*Cp(NS-1)));
    else
        Qnew(NS) = -B*Cv + sqrt((B*Cv)^2+2*Cv*Cp(NS-1));
    end

    Hnew(NS) = Cp(NS-1) - B*Qnew(NS);

    %---------------Values for plot-----------------%
    Hend(P) = Hnew(NS);
    Qend(P)=Qnew(NS);

    P = P + 1;
    Q = Qnew; %changing the variables for the next iteration
    H = Hnew;

    t=t+dt;
end

e_cpuT=cputime-cpuT;
disp(e_cpuT)
toc


figure(2)
plot(time,Hend)
grid on;
title(['Transient head just upstream valve a=', num2str(a,4)])
figure(3)
plot(time,Qend)
title('volume flow as a function of time')
axis([0 0.2*tend -Qend(1) Qend(1)]);
```

Matlab Script for MOC MIAB friction

```
close all
clear all
clc

tic
cpuT=cputime;


%---------------Defining Variables------------------%
N = 1001;       %grid boxes
a = 1319;       %wave propagation speed
Hr = 32;      %reservoir pressure head for BC
D = .0221;       %pipe diameter
A = .25*pi*D^2;       %crossectional area
g = 9.8066502;       %gravitational const 9.8066502
L = 37.23;       %Pipelength
f = .0345;       %Darcy-Weisbach friction factor
NS = N+1;        %number of grid points
tc = 0.009;        %closing time
tend = 1.5;
rho0 = 999.057;     %watrer density at 15.5 Celsius
dx = L/N;
dt = dx/a;
Nvector = 1:NS;
x = 0:dx:L;
%valve orifice
tau = 1;        %valve opening
t = 0;      %time in the beginning
Em = 1.5;       %taken from example in Streeter




%---------------Initial values------------------%
V0 = .1;
Q0(1:NS) = V0*A;
H0(1:NS) = Hr - f*dx*(Nvector-1).*Q0.*abs(Q0)/(2*g*A^2*D);
H00 = g*rho0*H0;        %Pressure head in Pa

figure(1)
subplot(2,1,1)
plot(x,H0);
title('initial pressure through pipe')
axis([0 L Hr*.999 Hr]);
```

```
subplot(2,1,2)
plot(x,Q0);
axis([0 L 0 Q0(1)*1.1]);
title('initial volume flow through pipe')

Q = Q0;
H = H0;
Qnew = zeros(1,NS);
Hnew = zeros(1,NS);

%----------Parrameters for MIAB Friction model---------------%
kx = .03;
kt = .04;
dt_ = zeros(1,N+1);
R = f*dx/(2*g*D*A^2);

%-----------------Time Variables-----------------------%
P =1;
timestep=1+floor((tend/dt));
time=linspace(0,tend,timestep);


for i = 0:dt:tend

    phi_p =sign(Q(2:NS).*(Q(2:NS)-(Q(1:NS-1)))/dx);
    phi_m =sign(Q(1:NS-1).*(Q(2:NS)-(Q(1:NS-1)))/dx);
    for j = 1:N
        if phi_p(j) == 0
            phi_p(j) = 1;
        end
        if phi_m(j) == 0
            phi_m(j) = 1;
        end
    end
    Bp = 2*a/(g*A)*(1+kt)./(-phi_p*kx + sqrt(kx^2 + 4*(1+kt)));
    Bm = 2*a/(g*A)*(1+kt)./(phi_m*kx + sqrt(kx^2 + 4*(1+kt)));

    alpha_p = -phi_p*kx + sqrt(kx^2 + 4*(1+kt));
    alpha_m = phi_m*kx + sqrt(kx^2 + 4*(1+kt));

    %%%% Finding dx,dt,.... for interpolation
    dxp = 2*dx*alpha_m./(alpha_p+alpha_m);
    dxm = 2*dx - dxp;
    dt_(1) = -dx*alpha_m(1)/(-2*a);
    dt_(2:N+1) = (dxp.*alpha_p)/(2*a);
```

```
dx2p = dt*dxp./dt_(2:N+1);
dx2m = dt*dxm./dt_(1:N);

%%%% Finding H-,H+....
%-----------------Upstream Boundary----------------------%
if dt_(1) < dt
    Hm(1) = H(2) + (H(3)-H(2))*(dx2m(1)-dx)/dx;
    Qm(1) = Q(2) + (Q(3)-Q(2))*(dx2m(1)-dx)/dx;
elseif dt_(1) > dt
    Hm(1) = H(1) + (H(2)-H(1))*dx2p(1)/dx;
    Qm(1) = Q(1) + (Q(2)-Q(1))*dx2p(1)/dx;
else
    Hm(1) = H(2);
    Qm(1) = Q(2);
end
    %%% finne Qnew,Hnew(1) for finne Hp,Qp(1)
Cm(1) = Hm(1)-Bm(1)*Qm(1)+R*Qm(1)*abs(Qm(1));
Hnew(1) = Hr;
Qnew(1)=(Hnew(1)-Cm(1))/Bm(1);
if dx2p(1) > dx
    Hp(1) = Hr;
    Qp(1) = Q(1)+(Qnew(1)-Q(1))*(dt-dt_(2))/dt;
elseif dx2p(1)<dx
    Hp(1) = H(1) + (H(2)-H(1))*(dx-dx2p(1))/dx;
    Qp(1) = Q(1) + (Q(2)-Q(1))*(dx-dx2p(1))/dx;
else
    Hp(1)=Hr;
    Qp(1)=Q(1);
end
%-----------------Interior Points----------------------%
for k = 2:N-1
    if dx2p(k)>dx
        Hp(k)=H(k-1)+(H(k)-H(k-1))*(2*dx-dx2p(k))/dx;
        Qp(k)=Q(k-1)+(Q(k)-Q(k-1))*(2*dx-dx2p(k))/dx;
    elseif dx2p(k)<dx
        Hp(k)=H(k)+(H(k+1)-H(k))*(dx-dx2p(k))/dx;
        Qp(k)=Q(k)+(Q(k+1)-Q(k))*(dx-dx2p(k))/dx;
    else
        Hp(k) = H(k);
        Qp(k) = Q(k);
    end
    if dx2m(k)<dx
        Hm(k)=H(k)+(H(k+1)-H(k))*dx2m(k)/dx;
        Qm(k)=Q(k)+(Q(k+1)-Q(k))*dx2m(k)/dx;
    elseif dx2m(k)>dx
```

```
            Hm(k)=H(k+1)+(H(k+2)-H(k+1))*(dx2m(k)-dx)/dx;
            Qm(k)=Q(k+1)+(Q(k+2)-Q(k+1))*(dx2m(k)-dx)/dx;
        else
            Hm(k)=H(k+1);
            Qm(k)=Q(k+1);
        end
    end
    %-----------------Downstream Boundary----------------------%
    if dt_(N+1)<dt
        Hp(N)=H(N-1)+(H(N)-H(N-1))*(2*dx-dx2p(N))/dx;
        Qp(N)=Q(N-1)+(Q(N)-Q(N-1))*(2*dx-dx2p(N))/dx;
    elseif dt_(N+1)>dt
        Hp(N)=H(N)+(H(N+1)-H(N))*(dx-dx2p(N))/dx;
        Qp(N)=Q(N)+(Q(N+1)-Q(N))*(dx-dx2p(N))/dx;
    else
        Hp(N)=H(N);
        Qp(N)=Q(N);
    end
        %%% finne Qnew Hnew(N+1) for finne Hm Qm (N)
    Cp(N)=Hp(N)+Bp(N)*Qp(N)-R*Qp(N)*abs(Qp(N));
    if t <= tc
        tau=(1-(1/tc)*t)^Em;
    else
        tau=0;
    end
    Cv = (Q0(1)*tau)^2/(2*H0(NS));
    if (Bp(N)*Cv)^2+2*Cv*Cp(N)>=0
        Qnew(N+1)=-Bp(N)*Cv+sqrt(abs((Bp(N)*Cv)^2+2*Cv*Cp(N)));
    else
        Qnew(N+1)=-Bp(N)*Cv-sqrt(abs((Bp(N)*Cv)^2+2*Cv*Cp(N)));
    end
    Hnew(N+1)=Cp(N)-Bp(N)*Qnew(N+1);
    if dx2m(N)<dx
        Hm(N)=H(N)+(H(N+1)-H(N))*dx2m(N)/dx;
        Qm(N)=Q(N)+(Q(N+1)-Q(N))*dx2m(N)/dx;
    elseif dx2m(N)>dx
        Hm(N)=H(N+1)+(Hnew(N+1)-H(N+1))*(dt-dt_(N+1))/dt;
        Qm(N)=Q(N+1)+(Qnew(N+1)-Q(N+1))*(dt-dt_(N+1))/dt;
    else
        Hm(N)=H(N+1);
        Qm(N)=Q(N+1);
    end

    %-----------------Computing Qnew, Hnew----------------------%
    Cp = Hp + Bp.*Qp - R*Qp.*abs(Qp);
```

```
    Cm = Hm - Bm.*Qm + R*Qm.*abs(Qm);
    %interior points 2:N
    Qnew(2:N)=(Cp(1:N-1)-Cm(2:N))./(Bm(2:N)+Bp(1:N-1));
    Hnew(2:N)=Cp(1:N-1)-Bp(1:N-1).*Qnew(2:N);
    %Note: Boundaries already computed

    %disp(t);
    %-----------------Variables for plot----------------------%
    Hend(P) = Hnew(NS);
    Qend(P)=Qnew(NS);

    P = P + 1;
    Q = Qnew;
    H = Hnew;

    disp(i)
    t=t+dt;
end

e_cpuT=cputime-cpuT;
disp(e_cpuT)
toc


figure(2)
plot(time,Hend)
grid on;
title(['Transient head just upstream valve a=', num2str(a,4)])
figure(3)
plot(time,Qend)
title('volume flow as a function of time')
axis([0 0.2*tend -Qend(1) Qend(1)]);
```

Matlab Script for MOC Zielke's friction

```
close all
clear all
clc

tic
cpuT=cputime;

%---------------Defining Variables------------------%
N = 1001;       %grid boxes
a = 1319;       %wave propagation 1286 expremintal, 1319 mandair sim
Hr = 32;      %reservoir pressure head for BC
D = .0221;       %pipe diameter
A = .25*pi*D^2;       %crossectional area
g = 9.8066502;       %gravitational const 9.8066502
L = 37.23;       %Pipelength
f = .0345;       %Darcy-Weisbach friction factor
NS = N+1;        %number of grid points
tc = 0.009;        %closing time
tend = .5;
rho0 = 999.057;     %watrer density at 15.5 Celsius
dx = L/N;
dt = dx/a; %at the Courant boundary, could be smaller
nu = 1.18181818181818e-06;
timestep=1+floor((tend/dt));
time=linspace(0,tend,timestep);
Pmax=size(time);
Pmax=Pmax(2);

%valve orifice
tau = 1;        %valve opening
t = 0;      %time in the beginning
Em = 1.5;       %taken from example in Streeter


%---------------Parameters for Zielkes model------------------%
R = f*dx/(2*g*D*A^2);
B = a/(g*A);
Rc = 16*nu*dx/(g*A*D^2);
A_z = .5/sqrt(pi);
B_z = 210.08;       %laminar flow Vardy
Q_Z = zeros(round(tend/dt),NS);
h_u = zeros(1,NS);

%Weighting Function
```

```
tauZ=4*nu*time/((D)^2);
tauZ=tauZ+tauZ(2);
W=A_z*exp(-B_z*tauZ)./(sqrt(tauZ));


Nvector = 1:NS;
x = 0:dx:L;

%---------------Initial values-----------------%
V0 = .1;
Q0(1:NS) = V0*A;
H0(1:NS) = Hr - f*dx*(Nvector-1).*Q0.*abs(Q0)/(2*g*A^2*D);
H00 = g*rho0*H0;        %Pressure head in Pa

figure(1)
subplot(2,1,1)
plot(x,H0);
title('initial pressure through pipe')
axis([0 L Hr*.999 Hr]);
subplot(2,1,2)
plot(x,Q0);
axis([0 L 0 Q0(1)*1.1]);
title('initial volume flow through pipe')


Q = Q0;
H = H0;
Qnew = zeros(1,NS);
Hnew = zeros(1,NS);

P=1;

for i = 0:dt:tend
    %Parameters for Zielke
    Q_Z(P,:)=Q;
    for j=1:(P-1)
        h_u = h_u+(Q_Z(j+1,:)-Q_Z(j,:))*W(P-j);
    end
    h_u = Rc*h_u;

    %All Cp, Cv
    Cp = H(1:NS-1) + B*Q(1:NS-1) - R*Q(1:NS-1).*abs(Q(1:NS-1)) - h_u(1:N
    Cm = H(2:NS) - B*Q(2:NS) + R*Q(2:NS).*abs(Q(2:NS)) + +h_u(2:NS);

    %Interior points
```

```
    Hnew(2:NS-1) = .5*(Cp(1:NS-2)+Cm(2:NS-1));
    Qnew(2:NS-1) = (Hnew(2:NS-1)-Cm(2:NS-1))/B;

    %upper boundary
    Hnew(1) = Hr;
    Qnew(1) = (Hnew(1)-Cm(1))/B;

    if t <= tc
        tau=(1-(1/tc)*t)^Em;
    else
        tau=0;
    end


    %lower boundary
    Cv = (Q0(1)*tau)^2/(2*H0(NS));

    if B*Cv+2*Cp(NS-1) < 0
        Qnew(NS) = -B*Cv - sqrt(abs((B*Cv)^2+2*Cv*Cp(NS-1)));
    else
        Qnew(NS) = -B*Cv + sqrt((B*Cv)^2+2*Cv*Cp(NS-1));
    end

    Hnew(NS) = Cp(NS-1) - B*Qnew(NS);


    disp(i);
    %Values for plot
    Hend(P) = Hnew(NS);
    Qend(P)=Qnew(NS);
    Hmid(P) = Hnew(NS/2);
    hfmid(P)=h_u(NS/2);

    P = P + 1;
    Q = Qnew;
    H = Hnew;
    h_u = zeros(1,NS);

    t=t+dt;
end


e_cpuT=cputime-cpuT;
disp(e_cpuT)
toc
```

```
figure(2)
plot(time,Hend)
grid on;
title(['Transient head just upstream valve a=', num2str(a,4)])
figure(3)
plot(time,Qend)
title('volume flow as a function of time')
axis([0 0.2*tend -Qend(1) Qend(1)]);

figure(5)
hold on
plot(time,hfmid/max(hfmid))
plot(time,W/max(W))
xlim([0 .1])
title(['Unsteady Headloss at midpoint a=', num2str(a,4)])
```

Appendix E

The heat equation was used for all three friction models. The script will be the same for all friction models, but the file containing the source terms will be different.

Matlab Script for the Heat equation

```
    close all
clear all
clc

%------------Defining Variables-------------%
%spatial refinement
nx = 50;
D = .0221;
x = linspace(0,D/2,nx);
dx = x(2)-x(1);
%timevector
tend = 1.5;          %end time
N = 1001;        %grid boxes
a = 1319;        %wave propagation 1286 expremintal, 1319 mandair sim
L = 37.23;        %Pipelength
dt = (L/N)/a;
timestep=1+floor((tend/dt));
t=linspace(0,tend,timestep);
nt= size(t);
nt=nt(2);
m = 1;

Re = 1870;
rho0 = 999.057;
f = .0345;
A = .25*pi*D^2;
V0 = .1;
Q0 = V0*A;
nu = V0*D/Re;
mu= nu*rho0;
dpdx=f*rho0*V0^2/(2*D); %dpdz0 = 7.78259976244344; %different density?
```

```
%----------------Source term from MOC-------------------%
global S_QSfric
load('Sourceterm_QSfriction_n1001.mat')

%----------------Solving the equations-------------------%
sol = pdepe(m,@heatcyl,@heatic,@heatbc,x,t);
u = sol(:,:,1);
u_end = u(nt,:);
%---------------Heat Equation Parameters----------------%
Q = 2*pi*(sum((sol(nt,:).*x)*dx));
V = Q/A;

%------------------PLOTS-----------------------%
figure(1)
surf(x,t,u)
xlabel('x')
ylabel('t')
zlabel('u(x,t)')
view(2)

figure(2)
plot(t,sol(:,1))
xlabel('Time')
ylabel('Velocity u(0,t)')
title('Velocity change at center of disc')

figure(3)
plot(x,sol(nt,:))
xlabel('x')
ylabel('Velocity u(x) [m/s]')
title('Position from disc center')
%------------For 3D hastighetsprofil-------------%
n=300;
for i = 1:n+1
    X(i,:)=sin(2*pi*(i-1)/n)*x;
    Y(i,:)=cos(2*pi*(i-1)/n)*x;
    Z(i,:)=u_end;
end
figure(4)
surf(X,Y,Z)
xlabel('x')
ylabel('y')
zlabel('u(r)')
view(0,0)
```

```
%------------Heat Equation-------------%
function [c,f,s] = heatcyl(x,t,u,dudx)
global S_QSfric
dt=2.81977310028864e-05;
nu=1.18181818181818e-06;
t_col=1+round(t/dt);
disp(t);
c = 1/nu;
f = dudx;
s = S_QSfric(t_col,1002);
end

%------------Initial Conditions-------------%
function u0 = heatic(x)
load('initial_u_r50.mat')
nx = 50;
D = .0221;
P = round(x/(.5*D/(nx-1)));
disp(P);
u0 = u_init_r50(P+1);
end

%------------Boundary Conditions-------------%
function [pl,ql,pr,qr] = heatbc(xl,ul,xr,ur,t)
pl = 0; %ignored by solver since m=1
ql = 0; %ignored by solver since m=1
pr = ur;
qr = 0;
end
```

Appendix F

Governing Equations for Pipe Flow

The 1D model which will be presented later, are based on the governing equations for 1D pipe flow, namely, the momentum and continuity equations. The following section presents and derives these equations, which ultimately are modified into Allievi's equations.

Momentum Equation

The momentum equation describes change in the systems momentum resulting from the forces acting on it. In the following section, the momentum equation for 1D flow in a pipe is derived from a freebody diagram, Figure F1. Wylie and Streeter provide a more detailed derivation [5].

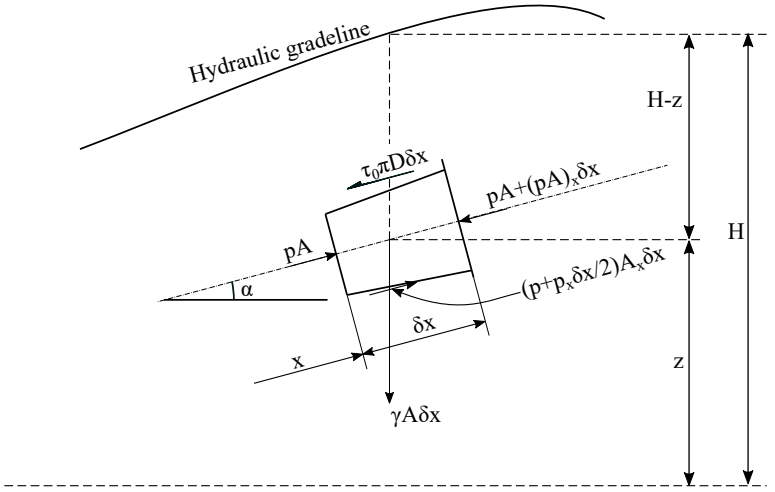

Figure F1: Freebody diagram showing the forces acting on a control volume

The equation is in terms of average velocity V, centerline pressure p, the discharge Q and the piezometric head H. Subscripts $_x$ and $_t$ denotes partial derivatives with respect to space and time.

The force balance related to the freebody diagram in Figure F1 is represented mathematically as

$$pA - [pA + (pA)_x \delta x] + \left(p + p_x \frac{\delta x}{2}\right) A_x \delta x - \tau_0 \pi D \delta x - \gamma A \delta x \sin\alpha = \rho A \delta x \dot{V}$$

Small terms containing δx^2 are dropped and the moment balance is reduced to

$$p_x A + \tau_0 \pi D + \rho g A \sin\alpha + \rho A \dot{V} = 0 \tag{F1}$$

For the sake of this derivation, the shear stress will be computed in terms of the Darcy-Weisbach friction factor. The transient calculations will then be determined from the current "steady" velocity. This way of modelling transient friction is often referred to as quasi-steady.

$$\tau_0 = \frac{\rho f V|V|}{8} \tag{F2}$$

f is the Darcy-Weisbach friction factor in the above equation. In Equation F1, $\dot{V}$ denotes the acceleration of a particle in fluid with the velocity, V. Its mathematical representation is below.

$$\dot{V} = VV_x + V_t \tag{F3}$$

Applying Equation F3 and Equation F2, Equation F1 becomes

$$\frac{p_x}{\rho} + VV_x + V_t + g\sin\alpha + f\frac{V|V|}{2D} = 0 \tag{F4}$$

The pressure term p can be related to the centerline elevation z, and the piezometric head H.

$$p_x = \rho g(H_x - \sin\alpha) \tag{F5}$$

Note Equation F5 is valid for liquids where the density ρ, is considered constant compared to H and z. It is not valid for gases.

Finally, using Equation F5, Equation F4 becomes

$$gH_x + VV_x + V_t + f\frac{V|V|}{2D} = 0 \tag{F6}$$

Continuity Equation

For 1D pipeflow where ρ is the density, A is the cross-sectional area and V is the cross-section average velocity, the continuity equation can be written in the following way

$$\frac{\partial(\rho A)}{\partial t} + \frac{\partial(\rho A V)}{\partial x} = 0 \tag{F7}$$

Introducing the material derivative, $\frac{D}{Dt} = \frac{\partial}{\partial t} + V\frac{\partial}{\partial x}$, and dividing Equation F7 by ρA, the equation becomes the following

$$\frac{1}{\rho A}\frac{D}{Dt}(\rho A) + V_x = 0 \tag{F8}$$

Using a dot to denote the material derivative, so that $\dot{A} = \frac{DA}{Dt}$, it can be written on the form

$$\frac{\dot{A}}{A} + \frac{\dot{\rho}}{\rho} + V_x = 0 \tag{F9}$$

In the next step, the following assumptions are listed below.

- The term $\dot{A}/A$ represents the expansion of the wall. The wall elasticity is negelcted by setting this term to 0
- Poison's ratio is introduced so that $\frac{\dot{\rho}}{\rho} = \frac{\dot{p}}{K}$
- The wave speed neglecting elasticity of pipe wall is $a = \sqrt{K/\rho}$

Applying these assumptions reduces Equation F9 to the following.

$$\frac{\dot{p}}{p} + a^2 V_x = 0 \tag{F10}$$

This form will be the same if the pipe wall elasticity is included, however the wave propagation speed, a, would be different. A thorough derivation of this is found in Wylie and Streeter. As for the momentum equation, the continuity equation is written in terms of the piezometric head.

$$\dot{p} = \rho g(\dot{H} - \dot{z}) = \rho g(V H_x + Ht - V z_x - z_t)$$

The pipe has no transverse motion so that $z_t = 0$ and $z_x = \sin\alpha$. Similar to Equation F1, α is the inclination angle of the pipe. Finally, we have Equation F11, the continuity equation, conveniently represented by the average velocity V and the piezometric head H.

$$V H_x + H_t - V \sin\alpha + \frac{a^2}{g} V_x = 0 \tag{F11}$$

Allievi's Equations

Both the momentum and continuity equations contains terms of lesser importance. Removing these terms leads to version of the momentum and continuity presented below. These are often referred to as Allievi's equations, and they govern transient behaviour of fluids in pipes. The method of characteristics (MOC) solves these equations to compute the transient properties of pipe flow. MOC will be thoroughly described in chapter 3.

$$g H_x + V_t + f\frac{V|V|}{2D} = 0 \tag{F12}$$

$$H_t + \frac{a^2}{g} V_x = 0 \tag{F13}$$